



Max-Planck-Institut für Meteorologie | Bundesstr. 53 | 20146 Hamburg

Dr. Vivek Arora  
Earth System Dynamics  
Copernicus Publications

**Alexander Winkler**

The Land in the Earth System  
Max-Planck-Institut für Meteorologie  
Bundesstr. 53  
20146 Hamburg  
Deutschland  
Tel.: +49 - (0)40 - 41173 - 542

alexander.winkler@mpimet.mpg.de  
www.mpimet.mpg.de

Hamburg, den 06. June 2019

Dear Dr. Arora,

On behalf of my co-authors, I would like to resubmit the revised manuscript “esd-2018-71” titled “Investigating the Applicability of Emergent Constraints” for publication in Earth System Dynamics. All referee comments are addressed comprehensively with additional analyses and revisions to the manuscripts, as described in the attached point-by-point response files.

Please find below the revised manuscript in marked-up version with revisions highlighted in red and blue.

Thank you for your consideration.

Yours sincerely,

  
Alexander Winkler (for all co-authors)

# ~~Limitations Investigating the Applicability of Emergent Constraints on Multi-Model Projections: Case Study of Constraining Vegetation Productivity With Observed Greening Sensitivity~~

Alexander J. Winkler<sup>1,2</sup>, Ranga B. Myneni<sup>3</sup>, and Victor Brovkin<sup>1</sup>

<sup>1</sup>Max Planck Institute for Meteorology, Bundesstrasse 53, 20146 Hamburg, Germany

<sup>2</sup>International Max Planck Research School on Earth System Modelling, Bundesstrasse 53, 20146 Hamburg, Germany

<sup>3</sup>Department of Earth and Environment, Boston University, Boston, Massachusetts 02215, USA

**Correspondence:** Alexander J. Winkler (alexander.winkler@mpimet.mpg.de)

## 1 Abstract.

2 Recent research on Emergent Constraints (EC) has delivered promising results in narrowing down uncertainty in climate  
3 predictions. The method utilizes a measurable variable (predictor) from the recent historical past to obtain a constrained es-  
4 timate of change in ~~a difficult-to-measure variable~~ an entity of interest (predictand) at a potential future CO<sub>2</sub> concentration  
5 (forcing) from multi-model projections. This procedure critically depends on, first, accurate estimation of the predictor from  
6 observations and models, and second, on a robust relationship between inter-model variations in the predictor-predictand space.  
7 ~~We Here, we~~ investigate issues related to these two themes in ~~this article, using a carbon cycle case study using observed~~ veg-  
8 etation greening sensitivity to ~~forcing during the satellite era~~ CO<sub>2</sub> forcing as a predictor of change in photosynthesis (Gross  
9 Primary Productivity) ~~of the Northern High Latitudes region (60° N–90° N, NHL), GPP~~ for a doubling of pre-industrial  
10 ~~concentration in the atmosphere~~ CO<sub>2</sub> concentration. Greening sensitivity is defined as changes in annual maximum of green leaf  
11 area index (LAI<sub>max</sub>) per unit CO<sub>2</sub> forcing realized through its radiative and fertilization effects. We first address the question  
12 of how to realistically characterize the greening sensitivity predictor of a large area ~~, the NHL, (e.g. greening sensitivity in the~~  
13 northern high latitudes region) from pixel-level LAI<sub>max</sub> data. This requires an investigation into uncertainties in LAI<sub>max</sub> ~~the~~  
14 observational data source and an evaluation of the spatial and temporal variability in greening sensitivity to forcing the predictor  
15 in both the data and model simulations. Second, the relationship between greening sensitivity and ΔGPP predictor-predictand  
16 relationship across the model ensemble depends on a strong coupling ~~among~~ between the two variables, i.e. simultaneous  
17 changes in GPP and LAI<sub>max</sub>. This coupling depends in a complex manner on the magnitude (level), time-rate of application  
18 (scenarios) and effects (radiative and/or fertilization) of CO<sub>2</sub> forcing. We investigate how each one of these three aspects of  
19 forcing can impair the EC estimate of the predictand (ΔGPP). ~~Accounting for uncertainties in greening sensitivity and stability~~  
20 ~~of the relation between inter-model variations results in a quantitative estimate of~~ Our results show that uncertainties in the  
21 ~~uncertainty (± 0.2 Pg C yr<sup>-1</sup>) on constrained GPP enhancement (ΔGPP = +3.4 Pg C yr<sup>-1</sup>) for a doubling of pre-industrial~~  
22 ~~atmospheric concentration in NHL. This ΔGPP is 60% larger than the conventionally used average of model projections.~~  
23 ~~The illustrated EC method can primarily originate from a lack of predictor comparability between models and observations,~~  
24 temporal variability, and the observational data source of the predictor. The disagreement between models on the mechanistic

1 behavior of the system under intensifying forcing limits the EC applicability. The here illustrated limitations and sources of  
2 uncertainty ~~and limitations of in~~ the EC method go beyond carbon cycle research and are generally ~~relevant for~~ applicable in  
3 Earth system sciences.

4 *Copyright statement.*

## 1 1 Introduction

2 Earth system models (ESMs) are powerful tools to predict ~~response~~ responses to a variety of forcings such as increasing atmo-  
3 spheric concentration of greenhouse gases and other agents of radiative forcing (Klein and Hall, 2015). Still, longterm ESM  
4 projections of climate change ~~can~~ have substantial uncertainties. This can be due to poorly understood processes in some cases,  
5 and in others, to missing or simplified representations called parameterizations (Flato et al., 2013; Klein and Hall, 2015; Knutti  
6 et al., 2017). Certain important processes, especially in the atmosphere, happen at spatial scales finer than can be possibly repre-  
7 sented in current ESMs. Consequently, ~~certain key aspects of the system, such as variability,~~ various phenomena in the system  
8 ranging from local extreme precipitation events ~~and to~~ large-scale climate modes, can be poorly simulated (Flato et al., 2013).  
9 Errors propagate and can be amplified through feedbacks among interacting components in the Earth system, resulting in biases  
10 whose origins can be difficult to identify (Flato et al., 2013). Furthermore, an inherent component of the Earth climatic sys-  
11 tem, its internal natural variability, is complicated to represent and simulate in models (Flato et al., 2013; Klein and Hall, 2015).  
12

13 Model Intercomparison Projects ~~aim is to~~ explore these uncertainties by coordinating a wide range of simulation setups fo-  
14 cusing on internal variability, boundary conditions, parameterizations, etc. (~~Taylor et al., 2012; Eyring et al., 2016; Flato et al., 2013; Knutti~~  
15 (Taylor et al., 2012; Flato et al., 2013; Eyring et al., 2016; Knutti et al., 2017)). Models developed at various institutions are driven  
16 with the same forcing information (e.g. historical forcing) or with identical idealized boundary conditions. However, each mod-  
17 eling group decides which of the processes to consider and implement in their ESM. The conventional approach of handling  
18 these multi-model ensembles is to use unweighted ensemble averages (Knutti, 2010; Knutti et al., 2017). This assumes that the  
19 models are independent of one another and equally good at simulating the climate system (Flato et al., 2013; Knutti et al., 2017).  
20 The large spread between model projections suggests that this assumption is not valid. Therefore, alternate methods have been  
21 developed to extract results more accurate than multi-model averages (~~e.g., model weighting scheme based on performance and interdependence~~  
22 (e.g. model weighting scheme based on performance and interdependence, Knutti et al., 2017)). The concept of *Emergent Con-*  
23 *straints* arises in this context, namely, as a method to reduce uncertainty in ESM projections relying on historical simulations  
24 and observations (Hall and Qu, 2006; Boé et al., 2009; Cox et al., 2013; Klein and Hall, 2015; Cox et al., 2018).  
25

26 The two key parts of an Emergent Constraint (EC) based method are a linear relationship arising from the collective behavior  
27 of a multi-model ensemble and an observational estimate for imposing the said constraint (Fig. 1). The linear relationship is  
28 a physically (or physiologically) based correlation between inter-model variations in an observable entity of the contempo-  
29 rary climate system (*predictor*) and a projected variable (*predictand*) that is ~~usually~~ difficult to observe or not observable  
30 at all. Combining the emergent linear relationship with observations of the predictor sets a constraint on the predictand  
31 (~~Knutti et al., 2017; Klein and Hall, 2015; Cox et al., 2013; Flato et al., 2013~~) (Cox et al., 2013; Flato et al., 2013; Klein and Hall, 2015; K  
32 . Many such ECs have been identified and reported, as briefly summarized below.

33

1 ~~Hall and Qu (2006)~~ [Hall and Qu \(2006\)](#) proposed a constraint on projections of snow-albedo feedback based on the correla-  
2 tion between large inter-model variations in feedback strength of the current seasonal cycle. The EC was first established for the  
3 CMIP3 ensemble and confirmed for phase five of the Coupled Model Intercomparison Project (~~CMIP5~~) (~~Qu and Hall, 2014; Flato et al., 2013~~)  
4 ([CMIP5; Flato et al., 2013; Qu and Hall, 2014](#)). Several EC studies followed with the goal of reducing uncertainty in projec-  
5 tions of the cloud feedback under global warming, as reviewed by ~~Klein and Hall (2015)~~ [Klein and Hall \(2015\)](#). It is thought  
6 that erroneous representation of low-cloud feedback in ESMs contributes essentially to the large uncertainty in equilib-  
7 rium climate sensitivity (ECS, 1.5 to 5 K), i.e. warming for a doubling of pre-industrial atmospheric ~~concentration~~ (~~2×~~)  
8 (~~Klein and Hall, 2015; Sherwood et al., 2014~~) [CO<sub>2</sub> concentration \(2×CO<sub>2</sub>; Sherwood et al., 2014; Klein and Hall, 2015\)](#). Re-  
9 cently, ~~Cox et al. (2018)~~ [Cox et al. \(2018\)](#) presented a different approach to constrain ECS based on its relationship to variabil-  
10 ity of global temperatures during the recent historical warming period. They ~~report~~ [reported](#) a constrained ECS estimate of 2.8  
11 K for 2×[CO<sub>2</sub>](#) (66% confidence limits of 2.2 – 3.4 K).

12

13 The concept of EC also found its way into the field of carbon cycle projections. A series of studies analyzed the extent to  
14 which inter-annual atmospheric [CO<sub>2</sub>](#) variability can serve as a predictor of longterm temperature sensitivity of terrestrial tropi-  
15 cal carbon storage. ~~Cox et al. (2013) and Wenzel et al. (2014)~~ [Cox et al. \(2013\) and Wenzel et al. \(2014\)](#) reported an emergent  
16 linear relationship, although with different slopes for CMIP3 and CMIP5 ensembles, resulting in slightly divergent constrained  
17 estimates (CMIP3:  $-53 \pm 17$  [Pg C K<sup>-1</sup>](#), CMIP5:  $-44 \pm 14$  [Pg C K<sup>-1</sup>](#)). ~~Wang et al. (2014)~~ [Wang et al. \(2014\)](#) however  
18 were unable to detect a similar relationship between the proposed predictor and predictand. Recently, ~~Lian et al. (2018)~~  
19 [Lian et al. \(2018\)](#) presented an EC estimate of the global ratio of transpiration to total terrestrial evapotranspiration (T/ET),  
20 which is substantially higher ( $0.62 \pm 0.06$ ) than the unconstrained value ( $0.41 \pm 0.11$ ). For the marine tropical carbon cycle,  
21 ~~Kwiatkowski et al. (2017)~~ [Kwiatkowski et al. \(2017\)](#) identified an emergent relationship between the longterm sensitivity of  
22 tropical ocean net primary production (NPP) to rising sea surface temperature (SST) in the equatorial zone and the interannual  
23 sensitivity of NPP to El Niño/Southern Oscillation driven SST anomalies. Tropical NPP is projected to decrease by  $3 \pm 1\%$   
24 for 1 K increase in equatorial SST according to the observational constraint.

25

26 Similar results were reported for [modeled](#) extra-tropical terrestrial carbon fixation in a 2×[CO<sub>2</sub>](#) world. Plant productivity is  
27 expected to increase due to the fertilizing and radiative effects of rising atmospheric ~~concentration~~. ~~Wenzel et al. (2016)~~ [CO<sub>2</sub>](#)  
28 [concentration](#). [Wenzel et al. \(2016\)](#) focused on constraining the [CO<sub>2</sub>](#) fertilization effect on plant productivity in the northern  
29 high latitudes (60° N – 90° N, NHL) and the entire extra-tropical area in the northern hemisphere (30° N – 90° N) using  
30 the seasonal amplitude of longterm [CO<sub>2</sub>](#) measurements at different latitudes. They presented a linear relationship between  
31 the sensitivity of [CO<sub>2</sub>](#) amplitude to rising atmospheric [CO<sub>2</sub>](#) concentration and the relative increase in zonally averaged gross  
32 primary production (GPP) for 2×[CO<sub>2</sub>](#). The observed [CO<sub>2</sub>](#) amplitude sensitivities at respective stations provided a constraint  
33 on the strength of the [CO<sub>2</sub>](#) fertilization effect, namely  $37\% \pm 9\%$  and  $32\% \pm 9\%$  for the NHL and the extra-tropical region,  
34 respectively.

35

1 Focusing on the NHL, ~~Winkler et al. (2019)~~ investigated how both effects of CO<sub>2</sub> enhance plant productivity while assess-  
2 ing the feasibility of vegetation greenness changes as a constraint (Fig. 1). Enhanced GPP due to the physiological effect and  
3 ensuing climate warming is indirectly evident in large-scale increase in summer time green leaf area (Myneni et al., 1997a; Zhu  
4 et al., 2016). Historical CMIP5 simulations show that the maximum annual leaf area index (LAI<sub>max</sub>, leaf area per ground area)  
5 increases linearly with both ~~concentration and growing degree days (above 0°, GDD0)~~ CO<sub>2</sub> concentration and temperature  
6 in NHL. ~~To avoid redundancy from co-linearity between the two driver variables, but retain their underlying time-trend and~~  
7 ~~interannual variability, the dominant mode from a principal component analysis of and GDD0 was used as the proxy driver~~  
8 ~~(denoted ω). This greening sensitivity (i.e.  $\frac{\Delta \text{LAI}_{\text{max}}}{\Delta \omega}$ ) can be inferred for the overlapping historical period from simulations~~  
9 ~~and observations alike.~~ In all ESMs, changes in these changes in LAI<sub>max</sub> strongly correlate to changes in GPP arising from  
10 the combined radiative and physiological effects of ~~enrichment strongly correlate with changes in LAI<sub>max</sub> in the historical~~  
11 ~~simulations~~ CO<sub>2</sub> enrichment. Thus, the large variation in ~~modelled-modeled~~ historical LAI<sub>max</sub> sensitivities-responses to the  
12 effects of CO<sub>2</sub> linearly maps to variation in ΔGPP at 2×. ~~Hence, this CO<sub>2</sub> in the CMIP5 ensemble. This~~ linear relationship in  
13 inter-model ~~variation between ΔGPP at 2× and historical greening sensitivities allows using the observed sensitivity variations~~  
14 enables the usage of the observed longterm change in LAI<sub>max</sub> as an EC on ΔGPP at 2× in NHL (3.4 ± 0.2, Winkler et al.,  
15 2018). CO<sub>2</sub> in NHL (3.4 ± 0.2 Pg C yr<sup>-1</sup>; Winkler et al., 2019).

16  
17 The ~~EC method (Fig. 1) has its limitations.~~ robustness of these EC estimates is debated, mainly because the EC approach  
18 is susceptible to methodological inconsistencies. For example, ~~Cox et al. (2013), Wang et al. (2014) and Wenzel et al. (2015)~~  
19 Cox et al. (2013), Wang et al. (2014) and Wenzel et al. (2015) investigated on constraining future terrestrial tropical carbon  
20 storage using the same set of models and data. However, they arrived at different EC estimates and divergent conclusions.  
21 Some reasons for ~~the~~ failure and essential criteria ~~required for successful application~~ of the EC approach were described pre-  
22 viously (Bracegirdle and Stephenson, 2012b; Klein and Hall, 2015), but this list is far from complete. ~~The main focus thus far~~  
23 ~~has been on caveats establishing an emergent linear relationship in a multi-model ensemble. However, large uncertainty on the~~  
24 ~~constraint could result potentially from how the observational predictor is derived and compared to the modeled estimates.~~ To  
25 account for this gap in the literature, a detailed investigation and description of the EC method in terms of its potential sources  
26 of uncertainty and the range of applicability are needed.

27  
28 Here, we revisit the study of ~~Winkler et al. (2019)~~ and elaborate on key issues concerning ~~sources of uncertainty regarding~~  
29 ~~the constraint and applicability~~ the robustness of the EC method.

30 ~~Uncertainty on~~ Uncertainty of the constrained estimate depends on (a) observed predictor and (b) modeled relationship,  
31 aside from the goodness-of-fit of the latter (green shading in Fig. 1). As for (a), the source of observations is an obvious first  
32 line of inquiry (Sect. 3.1). Spatial aggregation of data and model simulations introduces uncertainties, as the EC method is  
33 applied on large areal values of predictor and predictand. This is the subject of Sect. 3.2. The observed and modeled predictors  
34 are from the historical period. The representativeness, duration and match between data and models all introduce an uncertainty  
35 related to variations in the temporal domain – these are explored in (Sect. 3.3). The yellow shading in Fig. 1 represents the

1 total uncertainty on observed predictor from these three fronts. Regarding (b), the modeled linear relation varies (grey shading  
2 in Fig. 1) depending on three attributes of the forcing, i.e.  $\text{CO}_2$  concentration change, its magnitude, rate and effect (Sect. 3.4  
3 and 3.5). Lessons learned from analyses along these lines are presented in the conclusion section at the end.  
4

## 1 2 Data and Methods

### 2 2.1 ~~Observational data sets~~ Remotely sensed leaf area index

#### 3 2.1.1 ~~Remotely sensed leaf area index~~

4 We used the recently updated version (V1) of the leaf area index ~~data set~~ dataset (LAI3g) developed by (Zhu et al., 2013). It  
5 was generated using an artificial neural network (ANN) and the latest version (third generation) of the Global Inventory Mod-  
6 eling and Mapping Studies group (GIMMS) Advanced Very High Resolution Radiometer (AVHRR) normalized difference  
7 vegetation index (NDVI) data (NDVI3g). The latter have been corrected for sensor degradation, inter-sensor differences, cloud  
8 cover, observational geometry effects due to satellite drift, Rayleigh scattering and stratospheric volcanic aerosols (Pinzon and  
9 Tucker, 2014). This ~~data set~~ dataset provides global and year-round LAI observations at 15-day (bi-monthly) temporal resolu-  
10 tion and 1/12 degree spatial resolution from July 1981 to December 2016. Currently, this is the only available record of such  
11 length.

12  
13 The quality of previous version (V0) of LAI3g ~~data set~~ dataset was evaluated through direct comparisons with ground  
14 measurements of LAI and indirectly with other satellite-data based LAI products, and also through statistical analysis with  
15 climatic variables, such as temperature and precipitation variability (Zhu et al., 2013). The LAI3gV0 ~~data set~~ dataset (and re-  
16 lated fraction vegetation-absorbed photosynthetically active radiation ~~data set~~ dataset) has been widely used in various studies  
17 (~~Anav et al., 2013; Forkel et al., 2016; Zhu et al., 2016; Mao et al., 2016; Mahowald et al., 2016; Piao et al., 2014; Poulter et al., 2014; Ke~~  
18 ~~(Anav et al., 2013; Piao et al., 2014; Poulter et al., 2014; Forkel et al., 2016; Zhu et al., 2016; Mao et al., 2016; Mahowald et al., 2016; Ke~~  
19 . The new version, LAI3gV1, used in our study is an update of that earlier version.

20  
21 We also utilized a more reliable but shorter ~~data set~~ dataset from the Moderate Resolution Imaging Spectroradiometer  
22 (MODIS) aboard the NASA's Terra satellite (Yan et al., 2016a, b). These data are well calibrated, cloud-screened and corrected  
23 for atmospheric effects, especially tropospheric aerosols. The sensor-platform is regularly adjusted to maintain a precise orbit.  
24 All algorithms, including the LAI algorithm, are physics-based, well-tested and currently producing sixth generation ~~data sets~~.  
25 ~~The data set~~ datasets. The dataset provides global and year-round LAI observations at 16-day (bi-monthly) temporal resolution  
26 and 0.05° spatial resolution from 2000 to 2016.

27  
28 Leaf area index is defined as the one-sided green leaf area per unit ground area in broadleaf canopies and as one-half the  
29 green needle surface area in needleleaf canopies in both observational and CMIP5 simulation ~~data sets~~ datasets. It is expressed  
30 in units of m<sup>2</sup> green leaf area per m<sup>2</sup> ground area. Leaf area changes can be represented either by changes in annual maximum  
31 LAI (~~LAI<sub>max</sub>~~) (~~Cook and Pau, 2013~~) (LAI<sub>max</sub>; Cook and Pau, 2013), or growing season average LAI. In this study, we use the  
32 former because of its ease and unambiguity, as the latter requires quantifying the start- and end-dates of the growing season,  
33 something that is difficult to do accurately in NHL (Park et al., 2016) with the low resolution model data. Further, LAI<sub>max</sub>, is



1 less influenced by cloudiness and noise; accordingly, it is most useful in investigations of long-term greening and browning  
2 trends. The drawback of  $LAI_{max}$ , is the saturation effect at high LAI values (Myneni et al., 2002). However, this is less of a  
3 problem in high latitudinal ecosystems which are less-densely vegetated, with  $LAI_{max}$ , values typically in the range of 2 to 3.

4  
5 The bi-monthly satellite ~~data-sets~~ datasets were merged to a monthly temporal resolution by averaging the two composites  
6 in the same month and bi-linearly remapped to the resolution of the applied reanalysis product ( $0.5^\circ \times 0.5^\circ$ , CRU TS4.01).

### 8 **2.1.1 Environmental driver variables**

## 9 **2.2 Environmental driver variables**

10 We use ~~temperature, precipitation and data~~ time series of temperature and CO<sub>2</sub> to derive the observed historical forcing (Sect.  
11 2.4) and climatologies of precipitation and temperature to calculate climatic regimes (Fig. 2). Monthly averages of near-surface  
12 air temperature and precipitation are from the latest version of the Climatic Research Unit Timeseries ~~data-set~~ dataset (CRU  
13 TS4.01). The global data are gridded to  $0.5^\circ \times 0.5^\circ$  resolution (~~?~~) (Harris et al., 2014). Global monthly means of atmospheric  
14 CO<sub>2</sub> concentration are from the GLOBALVIEW-CO2 product (obspack\_co2\_1\_GLOBALVIEWplus\_v2.1\_2016\_09\_02; for  
15 details see <https://doi.org/10.25925/20190520>) provided by the National Oceanic and Atmospheric Administration / Earth Sys-  
16 tem Research Laboratory (NOAA / ESRL).

### 18 **2.3 Earth system model simulations**

19 We analyzed recent climate-carbon simulations of seven ESMs participating in the fifth phase of the Coupled Model Inter-  
20 comparison Project, CMIP (Taylor et al., 2012). The model simulated data were obtained from the Earth System Grid Federa-  
21 tion, ESGF (<https://esgf-data.dkrz.de/projects/esgf-dkrz/>). Seven ESMs provide output for the variables of interest (GPP, CO<sub>2</sub>,  
22 LAI, and near-surface air temperature) for simulations titled esmHistorical, RCP4.5, RCP8.5, 1pctCO2, esmFixClim1, and  
23 esmFdbk1. It is the same set of models analyzed in ~~Wenzel et al. (2016) and ?~~ Wenzel et al. (2016) and Winkler et al. (2019).  
24 The individual model setups and components are illustrated in more detail in various studies, such as Arora et al. (2013); Wenzel et al. (2014)

25  
26  
27 The esmHistorical simulation spanned the period 1850 to 2005 and was driven by observed conditions such as solar forcing,  
28 emissions or concentrations of short-lived species and natural and anthropogenic aerosols or their precursors, land use, anthro-  
29 pogenic as well as volcanic influences on atmospheric composition. The models are forced by prescribed anthropogenic CO<sub>2</sub>  
30 emissions, rather than atmospheric ~~concentrations~~ CO<sub>2</sub> concentrations.

31

1 Several Representative Concentration Pathways (RCPs) have been formulated describing different trajectories of greenhouse  
2 gas emissions, air pollutant production and land use changes for the 21st century. These scenarios have been designed based  
3 on projections of human population growth, technological advancement and societal responses (van Vuuren et al., 2011; Tay-  
4 lor et al., 2012). We analyzed simulations forced with specified concentrations of a high emissions scenario (RCP8.5) and  
5 a medium mitigation scenario (RCP4.5) reaching a radiative forcing level of 8.5 and 4.5 W m<sup>-2</sup> at the end of the century,  
6 respectively. These simulations were initialized with the final state of the historical runs and spanned the period 2006 to 2100.

8 1pctCO2 is an idealized fully coupled carbon-climate simulation initialized from a steady state of the ~~preindustrial~~ pre-industrial  
9 control run and atmospheric CO<sub>2</sub> concentration prescribed to increase 1% yr<sup>-1</sup> until quadrupling of the ~~preindustrial~~ pre-industrial  
10 level. The simulations esmFixClim and esmFdbk ~~are set-up similar to the aim to disentangle the two carbon cycle feedbacks~~  
11 in response to rising CO<sub>2</sub> analogous to the 1pctCO2 ~~with the difference, that in esmFixClim (esmFdbk) only the radiative~~  
12 effect from increasing concentration is included ~~setup: In esmFixClim CO<sub>2</sub>-induced climate change is suppressed (i.e. radiation~~  
13 transfer model sees constant pre-industrial CO<sub>2</sub> level), while the carbon cycle ~~sees the preindustrial level (vice versa)~~ (Taylor et al., 2009, 20  
14 responds to increasing CO<sub>2</sub> concentration (vice versa for esmFdbk; Taylor et al., 2009, 2012; Arora et al., 2013).

## 16 2.4 Estimation of greening sensitivities

17 We largely follow the methodology detailed in ~~Winkler et al. (2019)~~ Winkler et al. (2019). For both model and observational data, the two-dimensional  
18 global fields of LAI and the driver variables are cropped according to different classification schemes ~~(namely, vegetation~~  
19 classes (Olson et al., 2001), climatic regimes, and latitudinal bands) ~~(namely, climatic regimes, latitudinal bands and vegetation classes; Ols~~  
20 . The aggregated values are area-weighted, averaged in space, and temporally reduced to annual estimates dependent on the  
21 variable: annual maximum LAI, annual average atmospheric CO<sub>2</sub> concentration, and growing degree days (GDD0, yearly ac-  
22 cumulated temperature of days where near-surface air temperature > 0° C).

24 We use a standard linear regression model to derive the ~~greening sensitivity. On a historical greening sensitivities in models~~  
25 and observations alike (for details see the Methods section Estimation of historical LAI<sub>max</sub> sensitivity in Winkler et al., 2019).  
26 On the global scale, LAI<sub>max</sub> is assumed to be a linear function of atmospheric CO<sub>2</sub> concentration. For the temperature-limited  
27 high northern latitudes, we also have to account for warming and include temperature as an additional driver. We do this us-  
28 ing GDD0. We derive the dominant mode (denoted  $\omega$ ) through ~~Through~~ a principal component analysis of (PCA) of CO<sub>2</sub> and  
29 GDD0 to we avoid redundancy from co-linearity between the two driver variables, but retain their underlying time-trend and in-  
30 terannual variability. Thus, NHL (for details see the Methods section Dimension reduction using principal component analysis in Winkler  
31 . In particular, the PCA is performed on large-scale aggregated values as well as on pixel level to investigate on spatial  
32 variations. We only retain the first principal component (denoted  $\omega$ ), which explains a large fraction of the variance in  
33 models and observations (for more details see Supplementary Table 1 in Winkler et al., 2019). Figure A1 depicts the temporal  
34 development of CO<sub>2</sub> and GDD0 as well as their principal component  $\omega$  for observations. For the NHL, LAI<sub>max</sub> is then formu-

1 lated as a linear function of the proxy driver time series  $\omega$  ([Winkler et al., 2019](#)). The best-fit gradients and associated standard  
2 errors of the linear regression model represent the  $LAI_{\max}$  sensitivities, or greening sensitivities, and their uncertainty esti-  
3 mates, respectively. ~~For variations of finer spatial scale, the greening sensitivity is similarly calculated at the pixel scale.~~  
4

### 1 3 Results and Discussion

2 There are two parts to the EC methodology (Fig. 41) – a statistically robust relationship between modeled matching pairs  
3 of predictor-predictand values and an observed value of the predictor. The predictors are from a representative historical pe-  
4 riod. The predictands are modeled changes in a variable of interest at ~~a potential future~~ another forcing state of the system  
5 ~~, typically one that is difficult to measure. (e.g. potential future).~~ The projection of the observed predictor on the modeled  
6 relation yields a constrained value of the predictand. A causal basis has to buttress the predictor-predictand relationship,  
7 else the EC method may be spurious. For example, meaningful coupling between concurrent changes in GPP and LAI<sub>max</sub>  
8 with increasing atmospheric CO<sub>2</sub> concentration underpins our specific case study in the NHL, i.e. some of the enhanced  
9 GPP due to rising CO<sub>2</sub> concentration is invested in additional green leaves by ~~the plants (Winkler et al., 2018).~~ This plants  
10 (Myneni et al., 1997a; Forkel et al., 2016; Zhu et al., 2016; Mao et al., 2016; Winkler et al., 2019). Supplementary Figure 1 in  
11 Winkler et al. (2019) illustrates the specifics of the causal link underlying this predictor-predictand relationship. This tight  
12 coupling assures an approximately constant ratio of predictand to predictor across the models within the ensemble, thus setting  
13 up the potential for deriving an EC estimate.

14 Uncertainty on the constrained estimate depends on the observed predictor and modeled relationship, aside from the goodness-  
15 of-fit of the latter (Fig. 41). These are detailed below.

16

#### 17 3.1 Uncertainty in Observed ~~Sensitivity~~ Predictor Due to Data Source

18 We investigate this observational uncertainty using LAI data from two different sources, AVHRR (1/12 degree) and MODIS  
19 (1/20 degree), and spatially aggregating these by broad vegetation classes, latitudinal bands and climatic regimes. The ob-  
20 served ~~large-area sensitivities~~ large-scale LAI<sub>max</sub> sensitivities to CO<sub>2</sub> forcing are always positive (greening), irrespective of  
21 the source data and the method of aggregation (Fig. 2, Tab. 1). ~~This indicates a net increase in green leaf area across the NHL~~  
22 ~~during the observational period, as reported previously (Myneni et al., 1997a; Zhu et al., 2016; Forkel et al., 2016).~~ Overall,  
23 MODIS based estimates have higher uncertainty because of the shorter length of the data record (17 years). The failure to reli-  
24 ably estimate ~~sensivities~~ sensitivities in tropical forests (also in the latitudinal band 30° S – 30° N, and in hot, wet and humid  
25 climatic regimes, see Tab. 1 and Fig. 2) is due to saturation of optical remote sensing data over dense vegetation (LAI<sub>max</sub> > 5)  
26 and problems associated with high aerosol content and ubiquitous cloudiness. In ~~general~~ other regions, the estimated sensitivi-  
27 ties are comparable across sensors and aggregation schemes ~~(e.g. for latitudinal band, in particular in the high latitudinal band~~  
28 ~~(> 60° N/S, AVHRR: (-, AVHRR: [3.4 ± 0.5]) × 10<sup>-3</sup>; MODIS: (-, MODIS: [3.6 ± 0.9]) × 10<sup>-3</sup>; LAI<sub>max</sub> m<sup>2</sup> m<sup>-2</sup> ppm<sup>-1</sup>~~  
29 ~~); However, there are three interesting exceptions. First, higher sensitivities are seen in croplands, which reflect management~~  
30 ~~effects (fertilizer application, irrigation etc.) in addition to effects (Fig. 2a, Tab. 1). Second, lower sensitivities are seen in~~  
31 ~~sparsely vegetated areas and biomes (low LAI<sub>max</sub>, ~1) which are due to nutritionally poor soils and /or inhospitable climatic~~  
32 ~~conditions. Third, similarly low sensitivities are seen in dry regimes where precipitation is limiting and in humid regimes where~~  
33 ~~temperature is limiting (Fig. 2c, Tab. 1). CO<sub>2</sub>).~~ This aligns with previous studies reporting a net increase in green leaf area

1 across the high latitudes during the observational period (Myneni et al., 1997b; Zhu et al., 2016; Forkel et al., 2016).

2

3 This analysis illustrates the applicability and limitations of using observed greening sensitivities to  $\text{CO}_2$  forcing as a con-  
4 straint on photosynthetic production. For example, data from both AVHRR and MODIS sensors provide a comparable estimate  
5 of greening sensitivity in the colder high latitudes (~~boreal forests and tundra vegetation classes~~) ~~where precipitation is generally~~  
6 ~~less than 1000 mm (Winkler et al., 2018). However, the remote sensing LAI data are not suitable for similar studies in areas~~  
7 ~~dominated by croplands and in the tropics for reasons stated above.~~ (boreal forests and tundra vegetation classes; Winkler et al., 2019)  
8 . In the lower latitudes, however, the discrepancies among the two sensors indicate a considerable observational uncertainty  
9 and thus no robust estimation of the observed predictor is possible.

10

### 11 3.2 Uncertainty in Sensitivities Due to Spatial Aggregation

12 We focus further analyses on the NHL region ( $> 60^\circ \text{ N}$ ; Fig. 2b) ~~only because data from both AVHRR and MODIS sensors yield~~  
13 ~~comparable spatially aggregated greening sensitivities in this region unlike elsewhere, as discussed in Sect. 3.1.~~ because of  
14 two reasons. First, the direct human impact (i.e. land management) can be neglected in the high latitudes, thus, we can assume  
15 that the observed changes reflect the response of natural ecosystems. Second, the observational evidence of an increased plant  
16 productivity in the recent decades is well established (e.g. Keeling et al., 1996; Myneni et al., 1997a; Graven et al., 2013; Forkel et al., 201  
17 – an important requisite in defining a robust predictor.

18

19 In addition to the physiological effect of  $\text{CO}_2$ , also warming plays a key role in controlling plant productivity of ~~these the~~  
20 NHL temperature-limited ecosystems, and thus, vegetation greenness. To avoid redundancy from co-linearity between  $\text{CO}_2$   
21 and GDD0, we reduce dimensionality by performing a principal component analysis of the two driver variables (Sect. 2.4).  
22 The resulting first principal component explains most of the variance and retains the trend and year-to-year fluctuations in both  
23  $\text{CO}_2$  and GDD0. Therefore, we obtain a proxy driver (hereafter denoted  $\omega$ ) that represents the overall forcing signal causing  
24 observed vegetation greenness changes in NHL. ~~(Fig. A1).~~ Accordingly, greening sensitivity for the entire NHL area is derived  
25 as response to  $\omega$ , the combined forcing signal of rising  $\text{CO}_2$  and warming. This procedure also enables a better comparability  
26 between observations and models because varying strengths of physiological and radiative effects of  $\text{CO}_2$  among models are  
27 taken into account (Sect. 3.3 – 3.5).

28

29 The vegetated landscape in the NHL region is heterogeneous, with boreal forests in the south, vast tundra grasslands to the  
30 north and shrublands in-between. The species within each of these broad vegetation classes respond differently to changes in  
31 key environmental factors. Even within a species, such responses might vary due to different boundary conditions, such as  
32 topography, soil fertility, micrometeorological conditions, etc. How this fine scale variation in greening sensitivity impacts the  
33 aggregated value is assessed below.

34

1 The distribution of greening sensitivities from all NHL pixels is slightly skewed towards the positive (blue histogram). The  
2 mean value of this distribution (blue dashed line) is comparable to the sensitivity estimate derived from the spatially-averaged  
3 NHL time series (yellow dashed line; Fig. 3). Based on the Mann-Kendall test ( $p > 0.1$ ), nearly over half the pixels (54%) show  
4 positive statistically significant trends (greening), while about 10% show browning trends (~~possibly due to disturbances; Goetz et al., 2005~~)  
5 (possibly due to disturbances; Goetz et al., 2005). The distribution of these statistically significant sensitivities (red histogram)  
6 therefore has two modes, a weak browning and a dominant greening mode, resulting in a substantially higher mean value  
7 (red dashed line) in comparison to the spatially-averaged estimate (yellow dashed line; Fig. 3). Thus, by taking into account  
8 the remaining 36% of non-significantly changing pixels (as in the NHL spatially-averaged estimate), an additional source of  
9 uncertainty is possibly introduced. The mean sensitivity value is, of course, higher when only pixels showing a greening trend  
10 are considered in the analysis (green dashed line; Fig. 3). These are the only areas in NHL that actually show a large increase  
11 in plant productivity and consequently significant changes in leaf area. ~~ESMs-~~

12

13 Model output of several ESMs (CMIP5) reveal similar pixel-level variation in both the predictor ( $LAI_{max}$  ~~sensitivity to~~  
14  $\omega$ , historical simulation; Sect. 2.3) and associated changes in GPP in the NHL (~~Anav et al., 2013, 2015~~), the predictand (GPP,  
15 1pctCO<sub>2</sub>; Sect. 2.3), although ESMs operate on much coarser resolution (Fig. A2; see also Anav et al., 2013, 2015). Due to the  
16 coupling of the predictor and predictand, the distribution of ~~all-pixel-estimates-pixels with significant changes~~ is approximately  
17 the same for the two variables ~~-(Fig. A2)~~. Accordingly, averaging the equally distributed estimates likely does not affect the  
18 predictor-predictand relationship in the model ensemble (Fig. 1). Consequently, if all spatial gridded data arrays are consis-  
19 tently processed to spatially-aggregated estimates, each predictand and predictor (observed and modeled) estimate contain a  
20 coherent component of spatial variations. In other words, considering browning and non-significant pixels results in a lower  
21 overall  $LAI_{max}$  sensitivity in NHL, which in turn leads to a lower constrained estimate of  $\Delta GPP$  in NHL. This is consistent  
22 with the underlying relationship between predictor and predictand. On a related note, ~~Bracegirdle and Stephenson (2012a)-~~  
23 Bracegirdle and Stephenson (2012a) suggest that this source of error is not significantly dependent on the spatial resolution  
24 when comparing model subsets from high to low resolution.

25

26 The above analysis informs that spatially-averaged estimates are approximations containing a random error component  
27 due to inclusion of data from insignificantly changing pixels and a systematic bias component from ~~browning-pixels-pixels~~  
28 of reversed sign. This uncertainty is relevant to the EC method, where the observed sensitivity decisively determines the con-  
29 strained estimate from the ensemble of ESM projections (~~?Kwiatkowski et al., 2017~~) (Kwiatkowski et al., 2017; Winkler et al., 2019)  
30 . However, if spatial variations are treated consistently as an inherent component of observations and models, the EC method  
31 is only slightly susceptible to this source of uncertainty.

32

### 1 3.3 Uncertainty ~~in Sensitivities~~ Due to Temporal Variations

2 We seek recourse to longterm CMIP5 ESM simulations covering the historical period 1850 to 2005 (Sect. 2.3) to assess  
3 temporal variation in the predictor variable, because of the shortness of observational record. Three representative models  
4 (CESM1-BGC, MIROC-ESM, and HadGEM2-ES) spanning ~~a broad the full~~ range of NHL greening ~~sensitivity sensitivities~~  
5 in the CMIP5 ensemble (~~Winkler et al., 2018~~) (~~Winkler et al., 2019~~) are selected for this analysis. For each model, LAI<sub>max</sub>  
6 sensitivity to  $\omega$  in moving windows of different lengths ~~are evaluated~~ (15, 30, and 45 years; Fig. 4 ~~) are evaluated and A3~~).  
7 The analysis reveals two crucial aspects that highlight how temporal variations impair comparability of the predictor variable  
8 between models and observations – an essential component of the EC approach.

9  
10 First, window locations of modeled and observed predictor variable have to match. If the forcing in the simulations is low, for  
11 example, as in the second half of the 19th century when CO<sub>2</sub> concentration was increasing slowly, inter-annual variability dom-  
12 inates and LAI<sub>max</sub> sensitivity cannot be accurately estimated irrespective of the window length (Fig. 4 and A3). With increasing  
13 forcing over time (rising yearly rate of CO<sub>2</sub> infusion, and consequently, the concentration), the signal-to-noise ratio increases  
14 and LAI<sub>max</sub> sensitivity to  $\omega$  estimation stabilizes, for example, as in the second half of the 20th century. Therefore, LAI<sub>max</sub>  
15 sensitivities estimated at different temporal locations result in non-comparable values and eventually a false constrained esti-  
16 mate (details in Sect. 3.4). As an example, modeled sensitivities based on a 30-year window centered on year 1900, when CO<sub>2</sub>  
17 level increased by 10 ppm, ~~with and~~ observed sensitivity estimated from a 30-year window centered on year 2000, when CO<sub>2</sub>  
18 level increased by 55 ppm, describe different states of the system and therefore should not be ~~used contrasted~~ in the EC method.

19  
20 Second, in addition to temporal location, also window lengths have to match between observations and models. For all three  
21 models, sensitivities estimated from 15-year chunks show high variability and thus, a 15-year record is perhaps too short to  
22 obtain robust estimates. The LAI<sub>max</sub> sensitivity estimation becomes more stable with strengthening forcing and increasing  
23 window length (Fig. 4 and A3). As a consequence, using short-term observed sensitivity as a constraint on long-term model  
24 projections results in an incorrect EC estimate. Hence, the MODIS sensor record is, on the one hand, too short and does not,  
25 on the other hand, overlap temporally with the historical CMIP5 forcing (~~Fig. 1~~). Therefore, it does not provide a ~~correct~~  
26 ~~observational constraint~~ robust predictor in this EC study.

### 28 3.4 Level and Time Rate of CO<sub>2</sub> Forcing

29 The EC method raises an obvious question – does it not implicitly assume that the key operative mechanisms underpinning the  
30 EC relation remain unchanged because a future system state is being predicted based on its past behavior? To be specific, we  
31 are attempting to predict GPP at a future point in time based on greening sensitivity inferred from the past. Does this not require  
32 the assumption that the key underlying relationship which makes this prediction possible, namely, a robust coupling between  
33 contemporaneous changes in GPP and LAI<sub>max</sub> remains unchanged from the past to the future? To address this question, we

1 resort to the CMIP5 idealized simulation (1pctCO2), where atmospheric  $\text{CO}_2$  concentration increases 1% annually, starting  
2 from a ~~preindustrial~~ pre-industrial level of 284 ppm until a quadruple of this value is reached (Sect. 2.3). We limit the analysis  
3 to the three models (CESM1-BGC, MIROC-ESM, and HadGEM2-ES) which bracket the full range of GPP enhancement and  
4  $\text{LAI}_{\text{max}}$  sensitivity in the original seven ~~ESM ensemble~~ (Winkler et al., 2018). ~~(Winkler et al., 2019)~~.

5  
6 The relationship between simultaneous changes in GPP and  $\text{LAI}_{\text{max}}$  remains linear for all CMIP5 models in the range  
7  $1 \times \text{CO}_2$  to  $2 \times \text{CO}_2$  (Fig. 5 and A4, Tab. 2). With concentration increasing beyond  $2 \times \text{CO}_2$ , all models show weakening correla-  
8 tion ( $R^2$ , Tab. 2) and decreasing slope ( $b$ , Tab. 2) of this relationship (Fig. 5 and A4), suggesting a saturating rate of allocation  
9 of additional GPP to new leaves at higher levels of  $\text{CO}_2$ . Consequently,  $\text{LAI}_{\text{max}}$  sensitivity to increasing  $\text{CO}_2$  and associated  
10 warming decreases. At and over  $4 \times \text{CO}_2$  (1140 ppm), a level unlikely to be seen in the near future, there appears to be no  
11 relationship between  $\Delta\text{GPP}$  and  $\Delta\text{LAI}_{\text{max}}$ . This raises the question as to what extent does the weakening of the relationship  
12 between the predictor and predictand ~~(Fig. 1) at higher concentration affects~~ in each model at higher  $\text{CO}_2$  concentrations affect  
13 the EC analysis ~~-(Fig. 1)~~. To shed light on this matter, we perform the following ~~Gedankenexperiment~~ thought experiment.

14  
15 Understanding the relationship and interplay between forcing (increasing  $\text{CO}_2$  concentration), predictor ( $\text{LAI}_{\text{max}}$  sensitiv-  
16 ity), and the predictand ( $\Delta\text{GPP}$ ) is key to evaluating the EC method. We conceive four possible scenarios of how the system  
17 might behave with increasing forcing. For simplicity, we assume linearly increasing ~~concentration, use LAI instead of  $\text{CO}_2$~~   
18 concentration, LAI represents  $\text{LAI}_{\text{max}}$ , and GPP refers to its annual value below (Fig. 6). The four scenarios are: *All linear, all*  
19 *non-linear* (saturation), and two *mixed linear / non-linear* cases (Tab. A1). We emulate a multi-model ensemble by applying  
20 different random parameterizations for the linear and saturation (the hyperbolic tangent function) responses of GPP to  $\text{CO}_2$   
21 and of LAI to GPP. One of these realizations is assumed to represent pseudo-observations (dashed lines, Fig. 56). We discuss  
22 one case in detail for illustrative purposes (No. 3, Tab. A1).

23  
24 In scenario 3,  $\Delta\text{GPP}$  increases linearly with increasing  $\text{CO}_2$  (Fig. 6a), while  $\Delta\text{LAI}/\Delta\text{GPP}$  saturates (Fig. 6b). The LAI sen-  
25 sitivity to  $\text{CO}_2$  weakens with increasing forcing (Fig. 6c) as a response to saturation of GPP allocation to leaf area. We derive  
26 LAI sensitivities to  $\text{CO}_2$  for three different periods ('past periods' in Fig. 6c) to constrain  $\Delta\text{GPP}$  at a much higher  $\text{CO}_2$  level  
27 ('projected period' in Fig. 6a). Next, we apply the EC method on these pseudo-projections of  $\Delta\text{GPP}$  relying on LAI sensitivi-  
28 ties derived from the three past periods (Fig. 6d). The EC method is applicable even at a low forcing level (past period 1) in this  
29 simplified scenario because we neglect stochastic internal variability of the system. The slope of emergent linear relationship  
30 increases (Fig. 6d) as modeled LAI sensitivities decrease with rising  $\text{CO}_2$  concentration (Fig. 6c). The observational constraint  
31 on future  $\Delta\text{GPP}$ , however, remains nearly the same, because pseudo-observed LAI sensitivity also weakens at higher  $\text{CO}_2$  lev-  
32 els (dashed lines, Fig. 6c, d). Thus, the three EC estimates of  $\Delta\text{GPP}$  are approximately identical (Fig. 6d) and independent of  
33 the forcing level during past periods. With intensified forcing, the relationship between predictor and predictand remains linear  
34 within the model ensemble, although their relationship becomes non-linear within each model and, crucially, in reality as well.  
35 In other words, as long as the models agree on the occurrence and ~~"timing" of saturation, changes in~~ strength of saturation for



1 given forcing, i.e. the dynamics of the system, the inter-model variations of predictor and predictand relate linearly within the  
2 ~~model ensemble.~~ ensemble (Fig. 6). The same behavior is also seen in the other three scenarios (Tab. A1; Fig. A5, A6).

3  
4 Nevertheless, with ever increasing forcing and associated steepening of the emergent linear relationship, the LAI sensitivity  
5 loses its explanatory power at some point because the linear relationship eventually lies within the observational uncertainty  
6 and no meaningful constraint can be derived. This and disagreement between models on system dynamics are ultimate limits  
7 of the EC method. Interestingly, we find that all CMIP5 models agree on the occurrence of saturation, but slightly disagree  
8 on the ~~timing of saturation.~~ strength of saturation for given CO<sub>2</sub> forcing (Fig. 5, A4, and Tab. 2). Further, we find that the  
9 'all non-linear' scenario best describes the dynamics of the system in the forcing range from  $1 \times \text{CO}_2$  to  $4 \times \text{CO}_2$ . However,  
10 the saturation of LAI to GPP happens at a lower CO<sub>2</sub> level than saturation of GPP to ~~(Fig. A6).~~ CO<sub>2</sub>. Still, inferences from  
11 interpretation of Case 3 (Fig. 6) are equally applicable.

12  
13 Results from the above ~~Gedankenexperiment~~ thought experiment also highlight the importance of matching window loca-  
14 tions and lengths between models and observations, as discussed earlier (Sect. 3.3). For instance, taking LAI sensitivity from  
15 past period 2 (green dashed line, Fig. 6d) as an observational constraint on the multi-model linear relationship based on past  
16 period 3 (red solid line, Fig. 6d), results in a significant overestimation of constrained  $\Delta\text{GPP}$  (intersection of the two lines, Fig.  
17 6d).

18  
19 The above analysis informs that the constrained GPP estimate at one future period (e.g.  $2 \times \text{CO}_2$ ) is nearly independent of  
20 the past periods from when the observational sensitivities are derived, for most realistic scenarios. Now, we evaluate the EC  
21 method where sensitivity from one past period is used to obtain constrained GPP estimates at different periods in ~~the a potential~~  
22 future, i.e. progressively farther down the time-line of a CO<sub>2</sub>-enriched world. We utilize the greening sensitivity derived from  
23 35 years of observed  $\text{LAI}_{\text{max}}$  data (AVHRR, Sect. 2.1.1) and apply the EC method to CMIP5 1pctCO2 simulations. The sen-  
24 sitivities in this case are due to forcing from both CO<sub>2</sub> increase and associated warming during the observational period (Sect.  
25 2.4). We seek constrained GPP estimates ~~at future~~ for the NHL at different CO<sub>2</sub> levels ( $2 \times \text{CO}_2$ ,  $3 \times \text{CO}_2$ , and  $4 \times \text{CO}_2$ ).

26  
27 ~~Winkler et al. (2019)~~ Winkler et al. (2019) previously reported a strong linear relationship between modeled contemporaneous changes in  $\text{LAI}_{\text{max}}$   
28 and GPP arising from the combined radiative and physiological effects of CO<sub>2</sub> enrichment until  $2 \times \text{CO}_2$  in the CMIP5 en-  
29 semble ~~(Fig. 5).~~ (Fig. 5). As a result, models with low  $\text{LAI}_{\text{max}}$  sensitivity to  $\omega$  project lower  $\Delta\text{GPP}$  for a given increment of CO<sub>2</sub>  
30 concentration, and *vice versa*. Thus, the large variation in modeled historical  $\text{LAI}_{\text{max}}$  sensitivities linearly maps to variation in  
31  $\Delta\text{GPP}$  at  $2 \times$  ~~(Winkler et al., 2018; blue line, Fig. 7a).~~ CO<sub>2</sub> (Winkler et al., 2019, blue line, Fig. 7a). At higher levels, such as  
32  $3 \times \text{CO}_2$  (green line,  $R^2 = 0.93$ ) and  $4 \times \text{CO}_2$  (red line,  $R^2 = 0.88$ ), this linear relationship within the model ensemble, while still  
33 present, weakens (Fig. 7a; Tab. 3). This is because the CMIP5 models do not agree on the ~~timing and magnitude~~ strength of  
34 the saturation effect at higher CO<sub>2</sub> levels (Fig. ~~7a5 and A4~~ 7a5 and A4). The increment in constrained GPP estimates for successive equal  
35 increments of CO<sub>2</sub> decreases due to the saturation effect in all CMIP5 models (dashed horizontal lines, Fig. 7a). For example,

1 the change in GPP between  $3 \times \text{CO}_2$  and  $4 \times \text{CO}_2$  ( $\Delta\text{GPP} \sim 1.06 \text{ Pg C yr}^{-1}$ , Tab. 3) is much lower than between  $2 \times \text{CO}_2$  and  
2  $3 \times \text{CO}_2$  ( $\Delta\text{GPP} \sim 2.34 \text{ Pg C yr}^{-1}$ , Tab. 3).

3

4 We have thus far focused on the magnitude of  $\text{CO}_2$  concentration change and not on the time rate of this change. For  
5 example, a given amount of change in  $\text{CO}_2$  concentration, say 200 ppm, can be realized over different time periods, say over  
6 a 100 or 150 years. The problem of varying rates of  $\text{CO}_2$  concentration change is implicitly encountered when ESMs are  
7 executed under different forcing scenarios, such as RCPs ~~(Sect. 2.3)~~. A question then arises whether the constrained **GPP**  
8 **predictand** estimate is independent of the time rate of  $\text{CO}_2$  concentration change and dependent only on the magnitude of  
9  $\text{CO}_2$  concentration change. To investigate this aspect of forcing, we extract GPP estimates at the same  $\text{CO}_2$  concentration (535  
10 ppm; final concentration in RCP4.5) from three simulations of different forcing rates and calculate the difference relative to a  
11 common initial  $\text{CO}_2$  concentration (380 ppm; initial concentration of RCP scenarios). Hence, the magnitude of the forcing is  
12 the same but applied over different durations (RCP4.5:  $\sim 90\text{yr}$ , RCP8.5:  $\sim 45\text{yr}$ , and 1pctCO2:  $\sim 30\text{yr}$ ). A clear majority of the  
13 CMIP5 models show substantial differences in  $\Delta\text{GPP}$  between the different pathways of  $\text{CO}_2$  forcing. In general, GPP changes  
14 are higher for lower time rates of  $\text{CO}_2$  forcing, i.e. forcing over longer time periods. As a consequence, the EC estimates of  
15  $\Delta\text{GPP}$  for the same increase in  $\text{CO}_2$  concentration are scenario-dependent (Fig. 7b; Tab. 3) – a counter-intuitive result. For  
16 instance,  $\Delta\text{GPP}$  in the **low-low- $\text{CO}_2$ -rate** scenario (RCP4.5:  $\Delta\text{GPP} \sim 2.84 \text{ Pg C yr}^{-1}$ , Tab. 3) is  $\sim 39\%$  (1pctCO2:  $\Delta\text{GPP}$   
17  $\sim 2.05 \text{ Pg C yr}^{-1}$ , Tab. 3) and  $\sim 20\%$  (RCP8.5:  $\Delta\text{GPP} \sim 2.38 \text{ Pg C yr}^{-1}$ , Tab. 3) higher than the **high-high- $\text{CO}_2$ -rate** scenarios  
18 for an increase of 155 ppm  $\text{CO}_2$ . This analysis suggests that the vegetation response to rising  $\text{CO}_2$  is pathway dependent, at  
19 least in the NHL. One of the reasons for this could be species compositional changes in scenarios of low forcing rates, i.e. over  
20 longer time frames. This novel result, however, requires a separate in-depth study.

### 21 **3.5 Effects of $\text{CO}_2$ Forcing**

22 Higher concentration of  $\text{CO}_2$  in the atmosphere stimulates plant productivity through the fertilization and radiative effects (Ne-  
23 mani et al., 2003; Leakey et al., 2009; Arora et al., 2011; Goll et al., 2017). The two effects can be disentangled in the model  
24 world by conducting simulations in a ' $\text{CO}_2$  fertilization effect only' (esmFixClim1) and a 'radiative effect only' (esmFdbk1)  
25 setup (Sect. 2.3). These are termed below as idealized model simulations. We investigate here whether historical runs and  
26 observations, which include both effects, can be used to constrain GPP changes in idealized CMIP5 simulations ~~(e.g. as in~~  
27 ~~Wenzel et al. (2016))~~ (e.g. as in Wenzel et al., 2016).

28

29 We find strong linear relationships between historical  $\text{LAI}_{\text{max}}$  sensitivity and  $\Delta\text{GPP}$  for  $2 \times \text{CO}_2$  in both idealized setups  
30 (esmFixClim1:  $R^2 = 0.92$ , esmFdbk1:  $R^2 = 0.98$ , Tab. 3, Fig. 7c). Consequently, this linear relationship is also pronounced for  
31 calculated sums of both effects for each model (esmFixClim1 + esmFdbk1:  $R^2 = 0.95$ , Tab. 3, Fig. 7c). This suggests that the  
32 two effects act additively on plant productivity and, thus, each effect can be simply expressed in terms of a scaling factor of  
33 the total GPP enhancement. Hence, the application of the EC method on idealized simulations using real world observations is

1 conceptually feasible.

2

3 Interestingly, the two effects contribute about the same to the general increase in GPP at  $2\times\text{CO}_2$  (esmFixClim1:  $\Delta\text{GPP}$   
4  $\sim 1.35 \text{ Pg C yr}^{-1}$ , esmFdbk1:  $\Delta\text{GPP} \sim 1.38 \text{ Pg C yr}^{-1}$ , Tab. 3, Fig. 7c). At higher concentrations, such as  $3\times\text{CO}_2$  and  $4\times\text{CO}_2$ ,  
5 the enhancement in GPP saturates in both idealized setups. However, the radiative effect becomes dominant relative to the  
6  $\text{CO}_2$  fertilization effect when  $\text{CO}_2$  concentration exceeds  $2\times\text{CO}_2$  (e.g. at  $4\times\text{CO}_2$  esmFixClim1:  $\Delta\text{GPP} \sim 2.42 \text{ Pg C yr}^{-1}$ ,  
7 esmFdbk1:  $\Delta\text{GPP} \sim 3.06 \text{ Pg C yr}^{-1}$ , Tab. 3). Therefore, we can expect that at some point in the future, NHL photosynthetic  
8 carbon fixation will benefit more from climate change (e.g. warming) than from the fertilizing effect of  $\text{CO}_2$ .

### 9 3.6 Uncertainties in the ~~multi-model ensemble~~ Multi-Model Ensemble

10 Besides methodological sources of uncertainty discussed above, the estimate of an EC may also be deficient due to inaccurate  
11 assumptions about the model ensemble. First, possible common systematic errors in a multi-model ensemble (i.e. the entire en-  
12 semble misses an unknown but for the future essential process) are implicitly omitted in the EC approach, however, could cause  
13 a general over- or underestimation of the constrained value (Bracegirdle and Stephenson, 2012b; Stephenson et al., 2012). Sec-  
14 ond, the set of forcing variables for historical simulations may be incomplete (i.e. not yet identified drivers of observed changes)  
15 and ~~, thus, thus~~ the comparability of observations and model simulations is limited (Flato et al., 2013). Third, the EC method  
16 can be overly sensitive to individual models of the ensemble, which has a bearing on the robustness of the constrained value  
17 (Bracegirdle and Stephenson, 2012b). ~~Bracegirdle and Stephenson (2012b)~~ Bracegirdle and Stephenson (2012b) proposed a  
18 diagnostic metric (Cook's distance) to test an ensemble for influential models. Fourth, the ~~assumption behind the~~ predictand-  
19 predictor relationship not only has to rely on a physical, but also on a logical connection within the model ensemble, ~~meaning~~  
20 ~~that the analyzed characteristic of the predictor variable (e. g. sensitivity to the forcing, or historical relative/absolute changes)~~  
21 ~~is causally linked to changes in the predictand variable.~~ For instance, ~~Wenzel et al. (2016) reported~~ Wenzel et al. (2016)  
22 established a linear relationship between relative changes in the predictand taking the initial state into account (changes in GPP  
23 for doubling of ~~, so changes~~  $\text{CO}_2$  relative to the ~~preindustrial state, and initial pre-industrial state), and a predictor neglecting~~  
24 the initial state (historical sensitivity of  $\text{CO}_2$  amplitude to rising ~~, so neglecting the initial state~~  $\text{CO}_2$ ). This statistical relationship  
25 can be spurious, because the model skill of simulating an accurate initial state and a plausible sensitivity to a forcing are not  
26 connected.

27 These issues are to be contemplated when establishing an EC estimate and evaluating its robustness.

## 28 4 Conclusions

29 An in-depth analysis of the EC method is illustrated in this article through its application to projections of change in NHL  
30 photosynthesis under conditions of rising atmospheric  $\text{CO}_2$  concentration. Key conclusions highlighting the functionality of  
31 the EC method are presented below.

32

1 The importance of how the observational predictor is obtained cannot be emphasized enough because ~~it essentially defines~~  
2 ~~the constrained estimate. Thus, considerable care is required when selecting and processing the observational datasets. The~~  
3 ~~LAI data products of both AVHRR and MODIS sensors provide comparable estimates of greening sensitivity in the colder~~  
4 ~~northern high latitudes (i. e. boreal forests and tundra vegetation classes). In these ecosystems, factors associated with GPP~~  
5 ~~enhancement from forcing and consequent investment in leaf area dominate. This is not the case in croplands and tropical~~  
6 ~~areas. Therefore, the use of greening sensitivity as an observational constraint is not feasible in regions where croplands and/or~~  
7 ~~tropical vegetation dominate.~~ EC method is particularly sensitive to observational uncertainty. The single observational estimate  
8 essentially determines the EC, whereas the emergent linear relationship is established based on a collection of multi-model  
9 estimates (each model gets 'one vote', however, some models might be more influential than others; Bracegirdle and Stephenson, 2012b)  
10 . Hence, the observational uncertainty has a much larger bearing on the EC than the uncertainty of each individual model. To  
11 overcome this source of uncertainty, various meaningful observations should be taken into consideration when establishing the  
12 observed predictor.

13  
14 Spatially aggregating observations and model output of different resolutions in the EC method ~~is~~ constitutes another source  
15 of uncertainty. ~~Regional estimates of greening sensitivity~~ Predictors and predictands expressed as regional estimates (e.g.  
16 area-weighted mean of the NHL) are approximations of complex fine-scale processes. Aggregation will inevitably introduce  
17 a random error component due to inclusion of data estimates from areas where ~~LAI the predictor~~ is not changing ~~and or~~ a  
18 systematic bias from areas where ~~LAI is decreasing (browning).~~ The the predictor has a reversed sign. Thus, the spatially-  
19 aggregated ~~greening sensitivity is variables are~~ meaningful only if most of the region is ~~greening in response to forcing.~~  
20 ~~However, in agreement about the response to CO<sub>2</sub> forcing (e.g. more than half of the NHL is greening with rising CO<sub>2</sub>).~~  
21 However, we find that the source of uncertainty related to spatial aggregation is of minor importance as long as spatial vari-  
22 ations in observations and models simulations are treated consistently, ~~this source of uncertainty is likely of minor importance.~~

23  
24 A large source of uncertainty is associated with temporal variability of the predictor variable ~~throughout the historical period.~~  
25 ~~The evaluation of greening sensitivity requires when comparing models and observations. Establishing a robust predictor~~  
26 ~~requires evaluating~~ temporal window lengths of sufficient duration ~~;(approximately 30 years; and location) and their locations~~  
27 along the forcing time line. ~~And, these~~ Both window length and location should match between models and observations in  
28 the EC method. For example, the analysis in ~~Wenzel et al. (2016)~~ Wenzel et al. (2016) might have yielded different results and  
29 conclusions if model and observational predictor sensitivities were temporally matched. ~~The~~ We find that the relevance of  
30 window length decreases with increasing and accelerating forcing, depending on the magnitude of natural/internal variability  
31 (signal-to-noise ratio) of the predictor variable.

32  
33 The level, effect and ~~duration of forcing time-rate of applied CO<sub>2</sub> forcing can~~ have a bearing on the linear relationship be-  
34 tween ~~GPP enhancement and predictor sensitivities~~ the predictand and predictor variables (Fig. 4). ~~For example 1).~~ In our case  
35 study, the relationship underpinning the EC method, namely, that between concurrent  $\Delta\text{GPP}$  and  $\Delta\text{LAI}_{\text{max}}$  ~~changes~~ changes

1 ~~non-linearly~~ with increasing forcing level (i.e. ~~saturation with rising CO<sub>2</sub>~~ concentration). ~~This relation breaks down.~~ The EC  
2 method can still be applied, because the CMIP5 models agree on the non-linear behavior of the system. However, at very high  
3 ~~concentrations~~ CO<sub>2</sub> concentrations the models diverge and this relation breaks down, at which point the EC method fails. The  
4 two dominant effects of rising CO<sub>2</sub> concentration on vegetation, namely, the fertilization and radiative effects, appear to be  
5 approximately additive in terms of GPP enhancement to ~~forcing~~ CO<sub>2</sub> forcing in the NHL. Therefore, the EC method can be  
6 applied to constrain estimates of GPP due to one or the other, or both the effects. The models, however, document a higher ra-  
7 diative effect than fertilization at high CO<sub>2</sub> concentrations, i.e.  $3 \times \text{CO}_2$  and higher. ~~An~~ Another intriguing conclusion from our  
8 analysis is that the time-rate of forcing has an effect on GPP changes, that is, the projected GPP enhancement to CO<sub>2</sub> forcing  
9 seems to be dependent on how the forcing is applied over time, as in different scenarios or RCPs. This aspect is presently not  
10 well understood and requires further study.

11

12 The ~~analyses and inferences presented in this article lead to the following concrete result. The uncertainty on EC estimate of~~  
13 ~~GPP enhancement in NHL ( $\Delta\text{GPP} = +3.4 \text{ Pg C yr}^{-1}$ ) for a doubling of pre-industrial atmospheric concentration is  $\pm 0.2 \text{ Pg}$~~   
14 ~~C yr<sup>-1</sup> (Winkler et al., 2018). This EC estimate is 60% larger than the conventionally used average of model projections~~  
15 ~~(44% higher at the global scale), leading ? to conclude that most CMIP5 models included in their analysis were largely~~  
16 ~~underestimating photosynthetic production.~~ EC framework is widely promoted as observation-based evaluation tool for climate  
17 projections, especially in the context of the nascent CMIP6 ensemble (Eyring et al., 2019; Hall et al., 2019). Previous EC  
18 studies, however, exclusively focused on predictor-predictand combinations which exhibit so-called existent ECs (Hall et al., 2019)  
19 , i.e. predictor and predictand are found to relate linearly across the ensemble. In the context of ESM evaluation, non-existent  
20 ECs, i.e. predictor and predictand are found to be unrelated in the ensemble, are equally important. Since predictor and  
21 predictand variables are premised on our mechanistic process understanding, non-existent ECs reveal a fundamental disagreement  
22 on the system dynamics among the models. This study encourages to scrutinize these system dynamics in the predictor-predictand  
23 space and also report such non-existent, yet expected, ECs in order to advance model development and evaluation.

24

25 Across different disciplines each EC and its set of predictor and predictand are unique to some extent and require an  
26 individual detailed examination. In this article, we ~~scrutinized~~ addressed general potential sources of uncertainty and limi-  
27 tations ~~of the applicability of the EC method. Our findings are illustrated by~~ in the EC method by the means of a case study in  
28 carbon cycle research, ~~however, are generally relevant and applicable.~~ Thus, the illustrated results are qualitatively transmissive  
29 to other sets of predictors and predictands and are generally relevant in Earth system sciences.

1 *Author contributions.* A.J.W. performed the analysis. All authors contributed ideas and to writing of the manuscript.

2 *Competing interests.* The authors declare that they have no conflict of interest.

3 *Acknowledgements.* We thankfully acknowledge T. Park and C. Chen for their help with remote sensing data. We thank G. Lasslop for  
4 reviewing the manuscript. R.B.M. thanks Alexander von Humboldt Foundation and NASA's Earth Science Division for funding support that  
5 made his participation possible in this research.

## 1 **References**

- 2 Anav, A., Friedlingstein, P., Kidston, M., Bopp, L., Ciais, P., Cox, P., Jones, C., Jung, M., Myneni, R., and Zhu, Z.: Evaluating the  
3 Land and Ocean Components of the Global Carbon Cycle in the CMIP5 Earth System Models, *Journal of Climate*, 26, 6801–6843,  
4 <https://doi.org/10.1175/JCLI-D-12-00417.1>, 2013.
- 5 Anav, A., Friedlingstein, P., Beer, C., Ciais, P., Harper, A., Jones, C., Murray-Tortarolo, G., Papale, D., Parazoo, N. C., Peylin, P., Piao, S.,  
6 Sitch, S., Viovy, N., Wiltshire, A., and Zhao, M.: Spatiotemporal Patterns of Terrestrial Gross Primary Production: A Review, *Reviews of*  
7 *Geophysics*, 53, 2015RG000483, <https://doi.org/10.1002/2015RG000483>, 2015.
- 8 Arora, V. K., Scinocca, J. F., Boer, G. J., Christian, J. R., Denman, K. L., Flato, G. M., Kharin, V. V., Lee, W. G., and Merryfield, W. J.:  
9 Carbon Emission Limits Required to Satisfy Future Representative Concentration Pathways of Greenhouse Gases, *Geophysical Research*  
10 *Letters*, 38, L05 805, <https://doi.org/10.1029/2010GL046270>, 2011.
- 11 Arora, V. K., Boer, G. J., Friedlingstein, P., Eby, M., Jones, C. D., Christian, J. R., Bonan, G., Bopp, L., Brovkin, V., Cadule, P., Hajima, T.,  
12 Ilyina, T., Lindsay, K., Tjiputra, J. F., and Wu, T.: Carbon–Concentration and Carbon–Climate Feedbacks in CMIP5 Earth System Models,  
13 *Journal of Climate*, 26, 5289–5314, <https://doi.org/10.1175/JCLI-D-12-00494.1>, 2013.
- 14 Boé, J., Hall, A., and Qu, X.: September Sea-Ice Cover in the Arctic Ocean Projected to Vanish by 2100, *Nature Geoscience*, 2, 341–343,  
15 <https://doi.org/10.1038/ngeo467>, 2009.
- 16 Bracegirdle, T. J. and Stephenson, D. B.: Higher Precision Estimates of Regional Polar Warming by Ensemble Regression of Climate Model  
17 Projections, *Climate Dynamics*, 39, 2805–2821, <https://doi.org/10.1007/s00382-012-1330-3>, 2012a.
- 18 Bracegirdle, T. J. and Stephenson, D. B.: On the Robustness of Emergent Constraints Used in Multimodel Climate Change Projections of  
19 Arctic Warming, *Journal of Climate*, 26, 669–678, <https://doi.org/10.1175/JCLI-D-12-00537.1>, 2012b.
- 20 Cook, B. I. and Pau, S.: A Global Assessment of Long-Term Greening and Browning Trends in Pasture Lands Using the GIMMS LAI3g  
21 Dataset, *Remote Sensing*, 5, 2492–2512, <https://doi.org/10.3390/rs5052492>, 2013.
- 22 Cox, P. M., Pearson, D., Booth, B. B., Friedlingstein, P., Huntingford, C., Jones, C. D., and Luke, C. M.: Sensitivity of Tropical Carbon to  
23 Climate Change Constrained by Carbon Dioxide Variability, *Nature*, 494, 341–344, <https://doi.org/10.1038/nature11882>, 2013.
- 24 Cox, P. M., Huntingford, C., and Williamson, M. S.: Emergent Constraint on Equilibrium Climate Sensitivity from Global Temperature  
25 Variability, *Nature*, 553, 319–322, <https://doi.org/10.1038/nature25450>, 2018.
- 26 Eyring, V., Bony, S., Meehl, G. A., Senior, C. A., Stevens, B., Stouffer, R. J., and Taylor, K. E.: Overview of the Coupled Model Intercompar-  
27 ison Project Phase 6 (CMIP6) Experimental Design and Organization, *Geosci. Model Dev.*, 9, 1937–1958, [https://doi.org/10.5194/gmd-](https://doi.org/10.5194/gmd-9-1937-2016)  
28 9-1937-2016, 2016.
- 29 Eyring, V., Cox, P. M., Flato, G. M., Gleckler, P. J., Abramowitz, G., Caldwell, P., Collins, W. D., Gier, B. K., Hall, A. D., Hoffman, F. M.,  
30 Hurtt, G. C., Jahn, A., Jones, C. D., Klein, S. A., Krasting, J. P., Kwiatkowski, L., Lorenz, R., Maloney, E., Meehl, G. A., Pendergrass,  
31 A. G., Pincus, R., Ruane, A. C., Russell, J. L., Sanderson, B. M., Santer, B. D., Sherwood, S. C., Simpson, I. R., Stouffer, R. J., and  
32 Williamson, M. S.: Taking Climate Model Evaluation to the next Level, *Nature Climate Change*, p. 1, [https://doi.org/10.1038/s41558-018-](https://doi.org/10.1038/s41558-018-0355-y)  
33 0355-y, 2019.
- 34 Flato, G., Marotzke, J., Abiodun, B., Braconnot, P., Chou, S., Collins, W., Cox, P., Driouech, F., Emori, S., Eyring, V., Forest, C., Gleckler,  
35 P., Guilyardi, E., Jakob, C., Kattsov, V., Reason, C., and Rummukainen, M.: Evaluation of Climate Models, in: *Climate Change 2013:*  
36 *The Physical Science Basis. Contribution of Working Group I to the Fifth Assessment Report of the Intergovernmental Panel on Climate*

1 Change, edited by Stocker, T., Qin, D., Plattner, G.-K., Tignor, M., Allen, S., Boschung, J., Nauels, A., Xia, Y., Bex, V., and Midgley, P.,  
2 pp. 741–866, Cambridge University Press, Cambridge, United Kingdom and New York, NY, USA, 2013.

3 Forkel, M., Carvalhais, N., Rödenbeck, C., Keeling, R., Heimann, M., Thonicke, K., Zaehle, S., and Reichstein, M.: En-  
4 hanced Seasonal CO<sub>2</sub> Exchange Caused by Amplified Plant Productivity in Northern Ecosystems, *Science*, 351, 696–699,  
5 <https://doi.org/10.1126/science.aac4971>, 2016.

6 Fritz, S., See, L., McCallum, I., You, L., Bun, A., Moltchanova, E., Duerauer, M., Albrecht, F., Schill, C., Perger, C., Havlik, P., Mosnier, A.,  
7 Thornton, P., Wood-Sichra, U., Herrero, M., Becker-Reshef, I., Justice, C., Hansen, M., Gong, P., Abdel Aziz, S., Cipriani, A., Cumani,  
8 R., Cecchi, G., Conchedda, G., Ferreira, S., Gomez, A., Haffani, M., Kayitakire, F., Malanding, J., Mueller, R., Newby, T., Nonguierma,  
9 A., Olusegun, A., Ortner, S., Rajak, D. R., Rocha, J., Schepaschenko, D., Schepaschenko, M., Terekhov, A., Tiangwa, A., Vancutsem, C.,  
10 Vintrou, E., Wenbin, W., van der Velde, M., Dunwoody, A., Kraxner, F., and Obersteiner, M.: Mapping Global Cropland and Field Size,  
11 *Global Change Biology*, 21, 1980–1992, <https://doi.org/10.1111/GCB.12838>, 2015.

12 Goetz, S. J., Bunn, A. G., Fiske, G. J., and Houghton, R. A.: Satellite-Observed Photosynthetic Trends across Boreal North America As-  
13 sociated with Climate and Fire Disturbance, *Proceedings of the National Academy of Sciences of the United States of America*, 102,  
14 13 521–13 525, <https://doi.org/10.1073/pnas.0506179102>, 2005.

15 Goll, D. S., Winkler, A. J., Raddatz, T., Dong, N., Prentice, I. C., Ciais, P., and Brovkin, V.: Carbon–Nitrogen Interactions in Idealized  
16 Simulations with JSBACH (Version 3.10), *Geosci. Model Dev.*, 10, 2009–2030, <https://doi.org/10.5194/gmd-10-2009-2017>, 2017.

17 Graven, H. D., Keeling, R. F., Piper, S. C., Patra, P. K., Stephens, B. B., Wofsy, S. C., Welp, L. R., Sweeney, C., Tans, P. P., Kelley, J. J.,  
18 Daube, B. C., Kort, E. A., Santoni, G. W., and Bent, J. D.: Enhanced Seasonal Exchange of CO<sub>2</sub> by Northern Ecosystems Since 1960,  
19 *Science*, 341, 1085–1089, <https://doi.org/10.1126/science.1239207>, 2013.

20 Hall, A. and Qu, X.: Using the Current Seasonal Cycle to Constrain Snow Albedo Feedback in Future Climate Change, *Geophysical Research*  
21 *Letters*, 33, L03 502, <https://doi.org/10.1029/2005GL025127>, 2006.

22 Hall, A., Cox, P., Huntingford, C., and Klein, S.: Progressing Emergent Constraints on Future Climate Change, *Nature Climate Change*, p. 1,  
23 <https://doi.org/10.1038/S41558-019-0436-6>, 2019.

24 Harris, I., Jones, P. D., Osborn, T. J., and Lister, D. H.: Updated High-Resolution Grids of Monthly Climatic Observations – the CRU TS3.10  
25 Dataset, *International Journal of Climatology*, 34, 623–642, <https://doi.org/10.1002/joc.3711>, 2014.

26 Keeling, C. D., Chin, J. F. S., and Whorf, T. P.: Increased Activity of Northern Vegetation Inferred from Atmospheric CO<sub>2</sub> Measurements,  
27 *Nature*, 382, 146–149, <https://doi.org/10.1038/382146a0>, 1996.

28 Keenan, T. F., Prentice, I. C., Canadell, J. G., Williams, C. A., Wang, H., Raupach, M., and Collatz, G. J.: Recent Pause  
29 in the Growth Rate of Atmospheric CO<sub>2</sub> Due to Enhanced Terrestrial Carbon Uptake, *Nature Communications*, 7, 13 428,  
30 <https://doi.org/10.1038/ncomms13428>, 2016.

31 Klein, S. A. and Hall, A.: Emergent Constraints for Cloud Feedbacks, *Current Climate Change Reports*, 1, 276–287,  
32 <https://doi.org/10.1007/s40641-015-0027-1>, 2015.

33 Knutti, R.: The End of Model Democracy?, *Climatic Change*, 102, 395–404, <https://doi.org/10.1007/s10584-010-9800-2>, 2010.

34 Knutti, R., Sedláček, J., Sanderson, B. M., Lorenz, R., Fischer, E. M., and Eyring, V.: A Climate Model Projection Weighting Scheme  
35 Accounting for Performance and Interdependence, *Geophysical Research Letters*, 44, 1909–1918, <https://doi.org/10.1002/2016GL072012>,  
36 2017.

37 Kwiatkowski, L., Bopp, L., Aumont, O., Ciais, P., Cox, P. M., Laufkötter, C., Li, Y., and Séférian, R.: Emergent Constraints on Projections of  
38 Declining Primary Production in the Tropical Oceans, *Nature Climate Change*, 7, 355–358, <https://doi.org/10.1038/nclimate3265>, 2017.



1 Leakey, A. D. B., Ainsworth, E. A., Bernacchi, C. J., Rogers, A., Long, S. P., and Ort, D. R.: Elevated CO<sub>2</sub> Effects on Plant  
2 Carbon, Nitrogen, and Water Relations: Six Important Lessons from FACE, *Journal of Experimental Botany*, 60, 2859–2876,  
3 <https://doi.org/10.1093/jxb/erp096>, 2009.

4 Lian, X., Piao, S., Huntingford, C., Li, Y., Zeng, Z., Wang, X., Ciais, P., McVicar, T. R., Peng, S., Ottlé, C., Yang, H., Yang, Y., Zhang, Y.,  
5 and Wang, T.: Partitioning Global Land Evapotranspiration Using CMIP5 Models Constrained by Observations, *Nature Climate Change*,  
6 8, 640–646, <https://doi.org/10.1038/s41558-018-0207-9>, 2018.

7 Mahowald, N., Lo, F., Zheng, Y., Harrison, L., Funk, C., Lombardozi, D., and Goodale, C.: Projections of Leaf Area Index in Earth System  
8 Models, *Earth Syst. Dynam.*, 7, 211–229, <https://doi.org/10.5194/esd-7-211-2016>, 2016.

9 Mao, J., Ribes, A., Yan, B., Shi, X., Thornton, P. E., Séférian, R., Ciais, P., Myneni, R. B., Douville, H., Piao, S., Zhu, Z., Dickinson,  
10 R. E., Dai, Y., Ricciuto, D. M., Jin, M., Hoffman, F. M., Wang, B., Huang, M., and Lian, X.: Human-Induced Greening of the Northern  
11 Extratropical Land Surface, *Nature Climate Change*, 6, 959–963, <https://doi.org/10.1038/nclimate3056>, 2016.

12 Myneni, R., Keeling, C. D., Tucker, C. J., Asrar, G., and Nemani, R. R.: Increased Plant Growth in the Northern High Latitudes from 1981  
13 to 1991, *Nature*, 386, 698–702, <https://doi.org/10.1038/386698a0>, 1997a.

14 Myneni, R., Ramakrishna, R., Nemani, R., and Running, S.: Estimation of Global Leaf Area Index and Absorbed Par Using Radiative  
15 Transfer Models, *IEEE Transactions on Geoscience and Remote Sensing*, 35, 1380–1393, <https://doi.org/10.1109/36.649788>, 1997b.

16 Myneni, R. B., Hoffman, S., Knyazikhin, Y., Privette, J. L., Glassy, J., Tian, Y., Wang, Y., Song, X., Zhang, Y., Smith, G. R., Lotsch, A., Friedl,  
17 M., Morisette, J. T., Votava, P., Nemani, R. R., and Running, S. W.: Global Products of Vegetation Leaf Area and Fraction Absorbed PAR  
18 from Year One of MODIS Data, *Remote Sensing of Environment*, 83, 214–231, [https://doi.org/10.1016/S0034-4257\(02\)00074-3](https://doi.org/10.1016/S0034-4257(02)00074-3), 2002.

19 Nemani, R. R., Keeling, C. D., Hashimoto, H., Jolly, W. M., Piper, S. C., Tucker, C. J., Myneni, R. B., and Running,  
20 S. W.: Climate-Driven Increases in Global Terrestrial Net Primary Production from 1982 to 1999, *Science*, 300, 1560–1563,  
21 <https://doi.org/10.1126/science.1082750>, 2003.

22 Olson, D. M., Dinerstein, E., Wikramanayake, E. D., Burgess, N. D., Powell, G. V. N., Underwood, E. C., D’amico, J. A., Itoua, I.,  
23 Strand, H. E., Morrison, J. C., Loucks, C. J., Allnutt, T. F., Ricketts, T. H., Kura, Y., Lamoreux, J. F., Wettengel, W. W., Hedao, P., and  
24 Kassem, K. R.: Terrestrial Ecoregions of the World: A New Map of Life on Earth, *BioScience*, 51, 933–938, [https://doi.org/10.1641/0006-3568\(2001\)051\[0933:TEOTWA\]2.0.CO;2](https://doi.org/10.1641/0006-3568(2001)051[0933:TEOTWA]2.0.CO;2), 2001.

26 Park, T., Ganguly, S., Tømmervik, H., Euskirchen, E. S., Høgda, K.-A., Karlsen, S. R., Brovkin, V., Nemani, R. R., and Myneni, R. B.:  
27 Changes in Growing Season Duration and Productivity of Northern Vegetation Inferred from Long-Term Remote Sensing Data, *Environ-  
28 mental Research Letters*, 11, 084 001, <https://doi.org/10.1088/1748-9326/11/8/084001>, 2016.

29 Piao, S., Nan, H., Huntingford, C., Ciais, P., Friedlingstein, P., Sitch, S., Peng, S., Ahlström, A., Canadell, J. G., Cong, N., Levis, S., Levy,  
30 P. E., Liu, L., Lomas, M. R., Mao, J., Myneni, R. B., Peylin, P., Poulter, B., Shi, X., Yin, G., Viovy, N., Wang, T., Wang, X., Zaehle,  
31 S., Zeng, N., Zeng, Z., and Chen, A.: Evidence for a Weakening Relationship between Interannual Temperature Variability and Northern  
32 Vegetation Activity, *Nature Communications*, 5, 5018, <https://doi.org/10.1038/ncomms6018>, 2014.

33 Pinzon, J. E. and Tucker, C. J.: A Non-Stationary 1981–2012 AVHRR NDVI3g Time Series, *Remote Sensing*, 6, 6929–6960,  
34 <https://doi.org/10.3390/rs6086929>, 2014.

35 Poulter, B., Frank, D., Ciais, P., Myneni, R. B., Andela, N., Bi, J., Broquet, G., Canadell, J. G., Chevallier, F., Liu, Y. Y., Running, S. W.,  
36 Sitch, S., and van der Werf, G. R.: Contribution of Semi-Arid Ecosystems to Interannual Variability of the Global Carbon Cycle, *Nature*,  
37 509, 600–603, <https://doi.org/10.1038/nature13376>, 2014.

1 Qu, X. and Hall, A.: On the Persistent Spread in Snow-Albedo Feedback, *Climate Dynamics*, 42, 69–81, [https://doi.org/10.1007/s00382-](https://doi.org/10.1007/s00382-013-1774-0)  
2 013-1774-0, 2014.

3 Sherwood, S. C., Bony, S., and Dufresne, J.-L.: Spread in Model Climate Sensitivity Traced to Atmospheric Convective Mixing, *Nature*, 505,  
4 37–42, <https://doi.org/10.1038/nature12829>, 2014.

5 Stephenson, D. B., Collins, M., Rougier, J. C., and Chandler, R. E.: Statistical Problems in the Probabilistic Prediction of Climate Change,  
6 *Environmetrics*, 23, 364–372, <https://doi.org/10.1002/env.2153>, 2012.

7 Taylor, K. E., Stouffer, R. J., and Meehl, G. A.: A Summary of the CMIP5 Experiment Design, *PCDMI Rep.*, p. 33, 2009.

8 Taylor, K. E., Stouffer, R. J., and Meehl, G. A.: An Overview of Cmp5 and the Experiment Design, *Bulletin of the American Meteorological*  
9 *Society*, 93, 485–498, <https://doi.org/10.1175/BAMS-D-11-00094.1>, 2012.

10 van Vuuren, D. P., Edmonds, J., Kainuma, M., Riahi, K., Thomson, A., Hibbard, K., Hurtt, G. C., Kram, T., Krey, V., Lamarque, J.-F., Masui,  
11 T., Meinshausen, M., Nakicenovic, N., Smith, S. J., and Rose, S. K.: The Representative Concentration Pathways: An Overview, *Climatic*  
12 *Change*, 109, 5–31, <https://doi.org/10.1007/s10584-011-0148-z>, 2011.

13 Wang, J., Zeng, N., Liu, Y., and Bao, Q.: To What Extent Can Interannual CO<sub>2</sub> Variability Constrain Carbon Cycle Sensitivity to Climate  
14 Change in CMIP5 Earth System Models?, *Geophysical Research Letters*, 41, 3535–3544, <https://doi.org/10.1002/2014GL060004>, 2014.

15 Wenzel, S., Cox, P. M., Eyring, V., and Friedlingstein, P.: Emergent Constraints on Climate-Carbon Cycle Feedbacks in the CMIP5 Earth  
16 System Models, *Journal of Geophysical Research: Biogeosciences*, 119, 794–807, <https://doi.org/10.1002/2013JG002591>, 2014.

17 Wenzel, S., Eyring, V., Gerber, E. P., and Karpechko, A. Y.: Constraining Future Summer Austral Jet Stream Positions in the CMIP5 Ensemble  
18 by Process-Oriented Multiple Diagnostic Regression, *Journal of Climate*, 29, 673–687, <https://doi.org/10.1175/JCLI-D-15-0412.1>, 2015.

19 Wenzel, S., Cox, P. M., Eyring, V., and Friedlingstein, P.: Projected Land Photosynthesis Constrained by Changes in the Seasonal Cycle of  
20 Atmospheric CO<sub>2</sub>, *Nature*, 538, 499–501, <https://doi.org/10.1038/nature19772>, 2016.

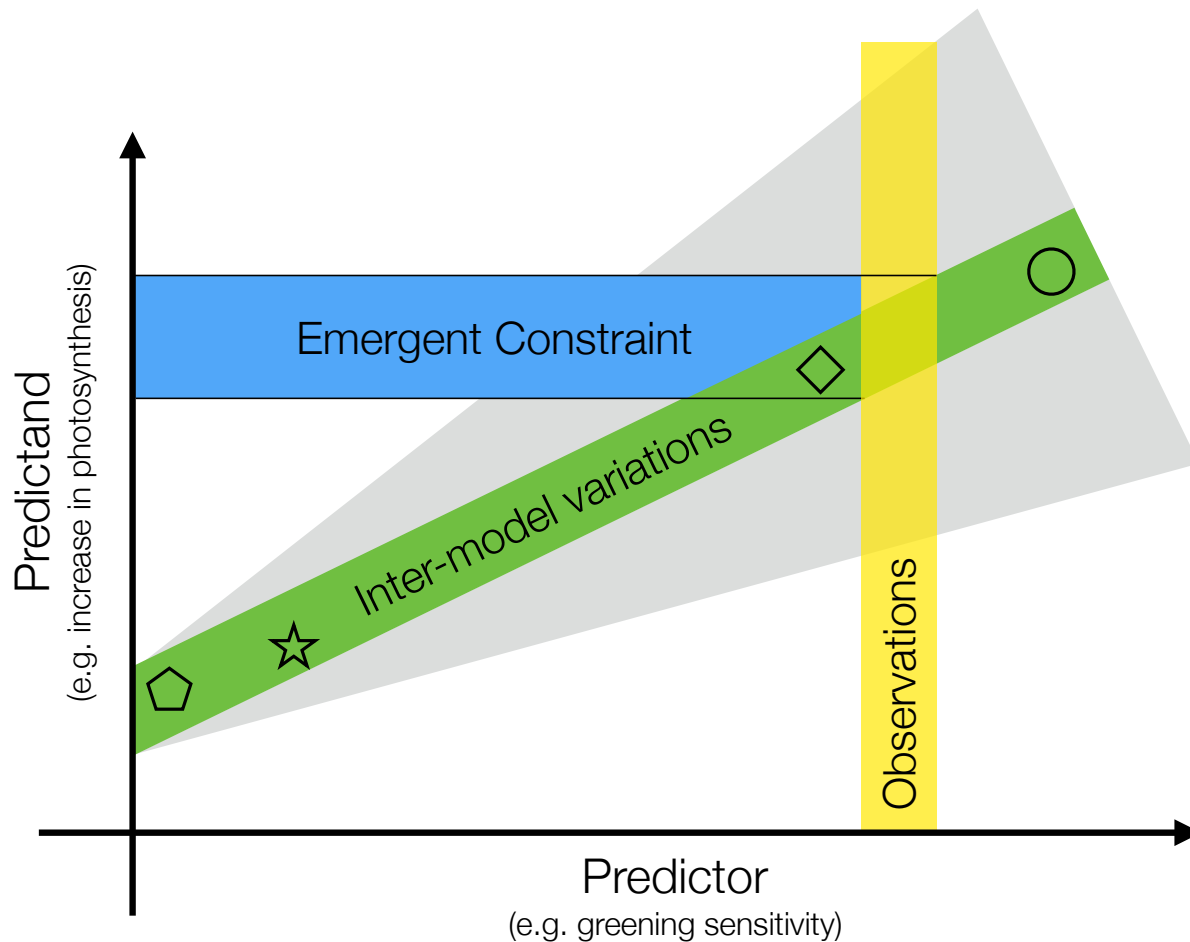
21 Winkler, A. J., Myneni, R. B., Alexandrov, G. A., and Brovkin, V.: Earth System Models Underestimate Carbon Fixation by Plants in the  
22 High Latitudes, *Nature Communications*, 10, 885, <https://doi.org/10.1038/S41467-019-08633-Z>, 2019.

23 Yan, K., Park, T., Yan, G., Chen, C., Yang, B., Liu, Z., Nemani, R. R., Knyazikhin, Y., and Myneni, R. B.: Evaluation of MODIS LAI/FPAR  
24 Product Collection 6. Part 1: Consistency and Improvements, *Remote Sensing*, 8, 359, <https://doi.org/10.3390/rs8050359>, 2016a.

25 Yan, K., Park, T., Yan, G., Liu, Z., Yang, B., Chen, C., Nemani, R. R., Knyazikhin, Y., and Myneni, R. B.: Evaluation of MODIS LAI/FPAR  
26 Product Collection 6. Part 2: Validation and Intercomparison, *Remote Sensing*, 8, 460, <https://doi.org/10.3390/rs8060460>, 2016b.

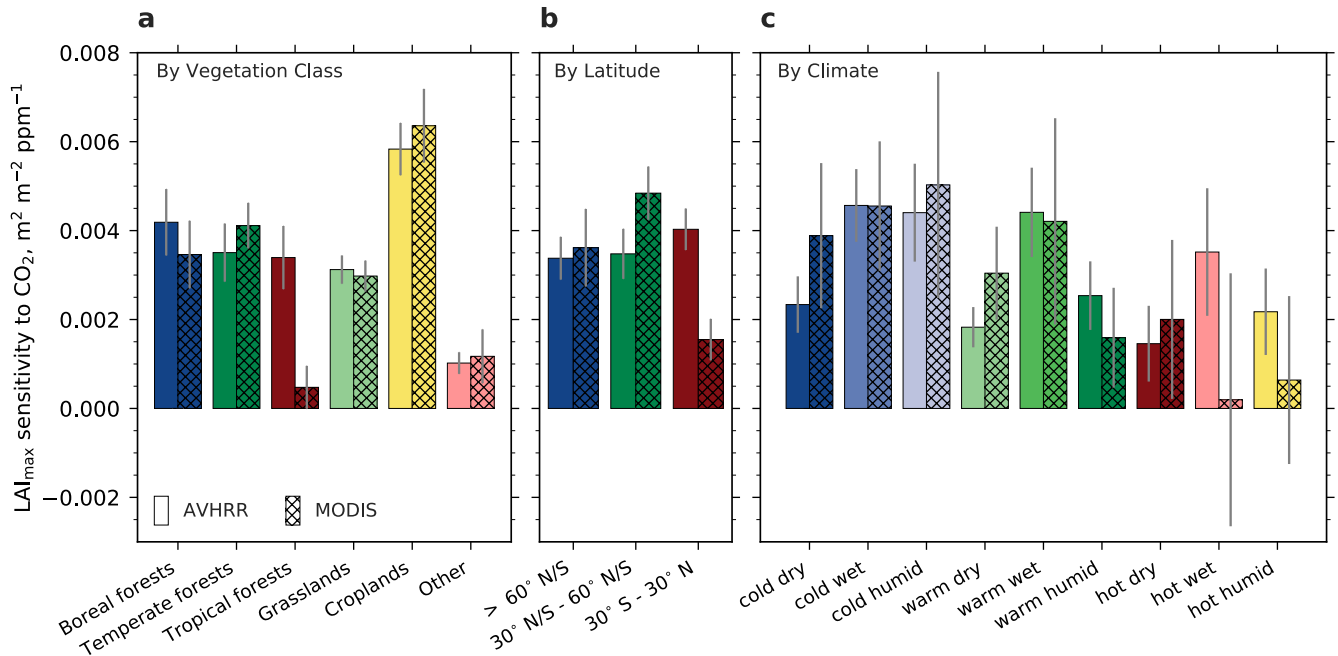
27 Zhu, Z., Bi, J., Pan, Y., Ganguly, S., Anav, A., Xu, L., Samanta, A., Piao, S., Nemani, R. R., and Myneni, R. B.: Global Data Sets of Vegetation  
28 Leaf Area Index (LAI)3g and Fraction of Photosynthetically Active Radiation (FPAR)3g Derived from Global Inventory Modeling and  
29 Mapping Studies (GIMMS) Normalized Difference Vegetation Index (NDVI3g) for the Period 1981 to 2011, *Remote Sensing*, 5, 927–948,  
30 <https://doi.org/10.3390/rs5020927>, 2013.

31 Zhu, Z., Piao, S., Myneni, R. B., Huang, M., Zeng, Z., Canadell, J. G., Ciais, P., Sitch, S., Friedlingstein, P., Arneth, A., Cao, C., Cheng,  
32 L., Kato, E., Koven, C., Li, Y., Lian, X., Liu, Y., Liu, R., Mao, J., Pan, Y., Peng, S., Peñuelas, J., Poulter, B., Pugh, T. A. M., Stocker,  
33 B. D., Viogy, N., Wang, X., Wang, Y., Xiao, Z., Yang, H., Zaehle, S., and Zeng, N.: Greening of the Earth and Its Drivers, *Nature Climate*  
34 *Change*, 6, 791–795, <https://doi.org/10.1038/nclimate3004>, 2016.



1

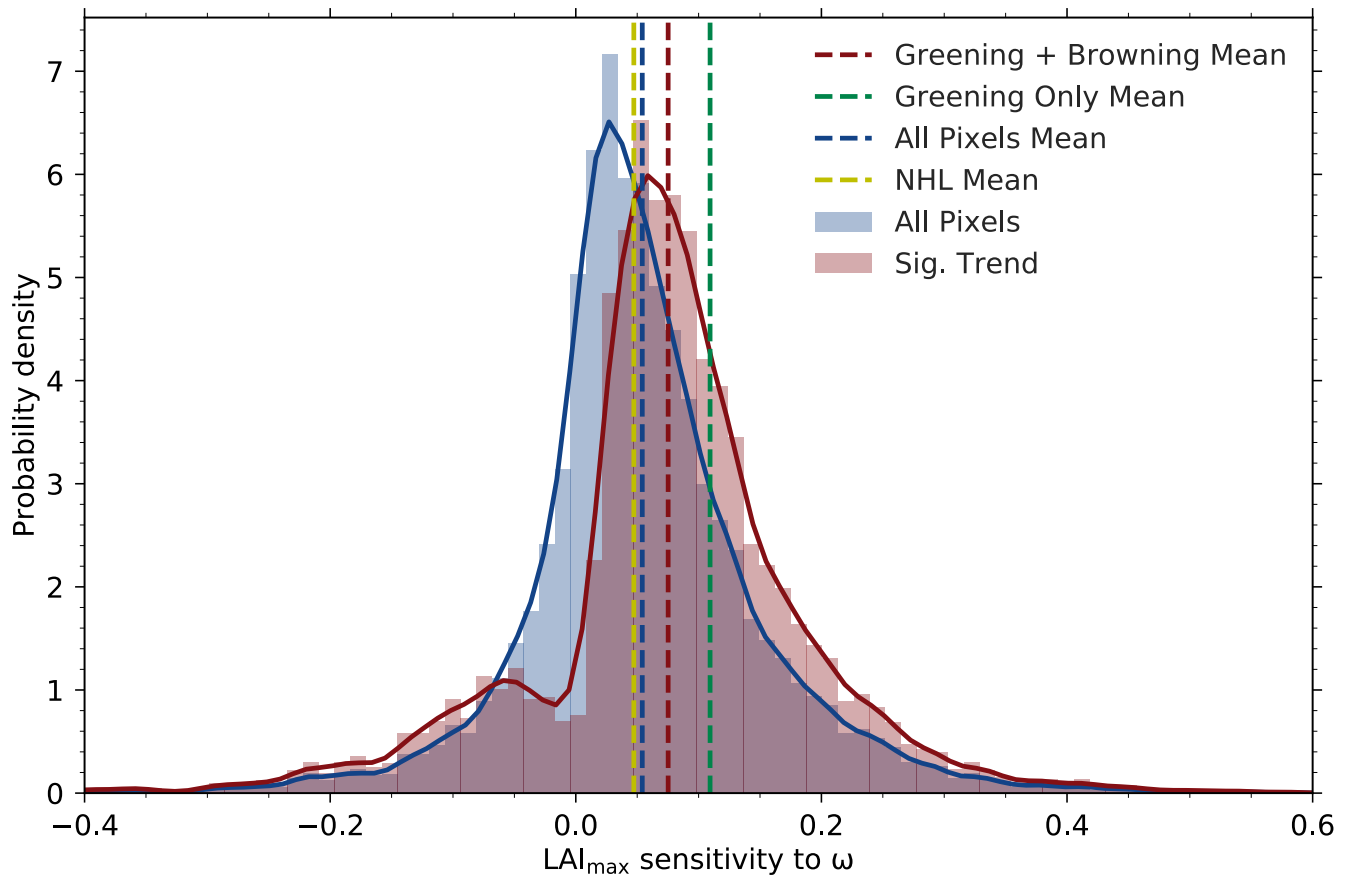
2 **Figure 1.** Schematic depiction of the Emergent Constraint (EC) method and factors affecting the uncertainty of the constrained estimate.  
3 The predictor ( $x$  axis) is change in annual maximum of green leaf area index ( $LAI_{max}$ ) due to unit forcing ( $CO_2$  increase and associated  
4 climatic changes) during a representative historical period. It is termed greening sensitivity in this study. The predictand ( $y$  axis) is projected  
5 changes in Gross Primary Productivity (GPP) in response to rising  $CO_2$  concentration (e.g. for a doubling of the pre-industrial level). Both  
6 the predictor and predictand refer to large area values, in this case, the entire ~~Norther~~Northern High Latitudes (NHL). Inter-model variations  
7 (each symbol represents a model) in matching pairs of predictor and predictand result in a linear relationship between the two (green band),  
8 i.e. the ratio (predictand/predictor) is approximately constant across the model ensemble. The slope depends on forcing attributes (gray  
9 shading), such as its level ( $CO_2$  concentration, Sect. 3.4), time rate of application (scenarios such as various RCPs, Sect. 3.4) and different  
10 effects (i.e. fertilization, radiative, etc., Sect. 3.5). The observed sensitivity (yellow vertical bar) is used to find the constrained estimate of  
11 the predictand (i.e. change in GPP). The ability to accurately estimate the predictor depends on the source of observational data (Sect. 3.1),  
12 and its spatial (Sect. 3.2) and temporal variability (Sect. 3.3). Observed (yellow bar) and modeled predictor values ( $x$  coordinate of symbols)  
13 must be obtained from matching time periods, i.e. at the same level of historical forcing, to ensure comparability (Sect. [3.3](#) and [3.4](#)). All  
14 these factors, together with the goodness-of-fit of inter-model variations (width of green shading), finally define the uncertainty of the derived  
15 constrained estimate (blue horizontal bar with black solid lines depicting the upper and lower bound of uncertainty).



1

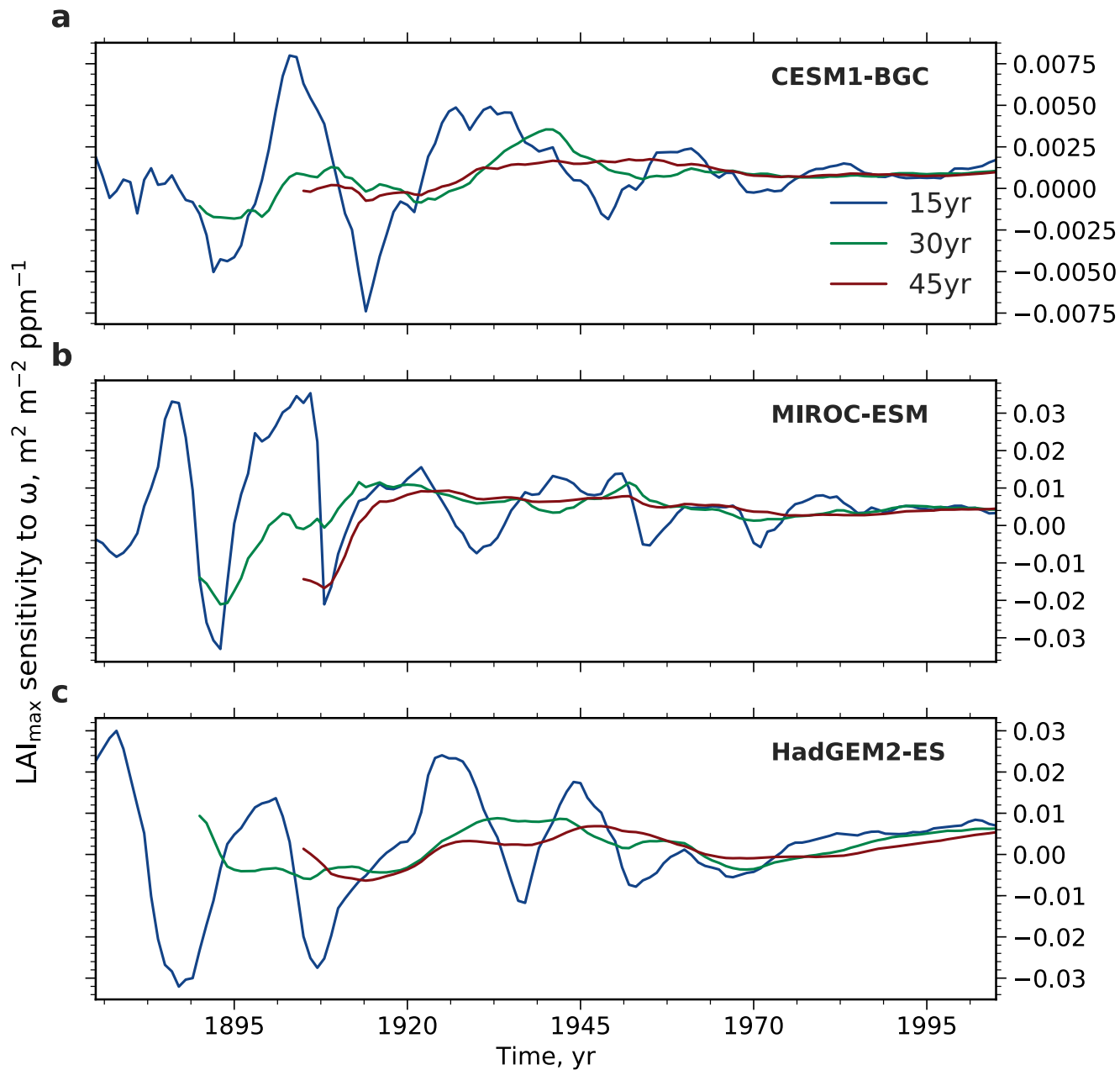
2

3 **Figure 2.** Bar charts showing regression slopes of LAI<sub>max</sub> against atmospheric CO<sub>2</sub> concentration for broad vegetation classes  
 4 (a: Olson et al., 2001; Fritz et al., 2015), Olson et al. (2001), latitudinal bands (b) and climate regimes (c). The class "Other" includes  
 5 deserts, mangroves, barren and urban land, snow and ice, and permanent wetlands. The climatic boundaries are defined as follows -  
 6 cold: < 10°C; warm: > 10°C & < 25°C; hot: > 25°C; dry: < 500 mm a<sup>-1</sup>; wet: > 500 mm a<sup>-1</sup> & < 1000 mm a<sup>-1</sup>; humid: > 1000  
 7 mm a<sup>-1</sup>. Sensitivities evaluated from data from two satellite-borne sensors are shown, AVHRR (1982–2016, Pinzon and Tucker (2014))  
 8 (1982–2016; Pinzon and Tucker, 2014) and MODIS (2000–2016, Yan et al. (2016a, b)) (2000–2016; Yan et al., 2016a, b). Grey bars in-  
 9 dicate the standard error of the best linear fit.



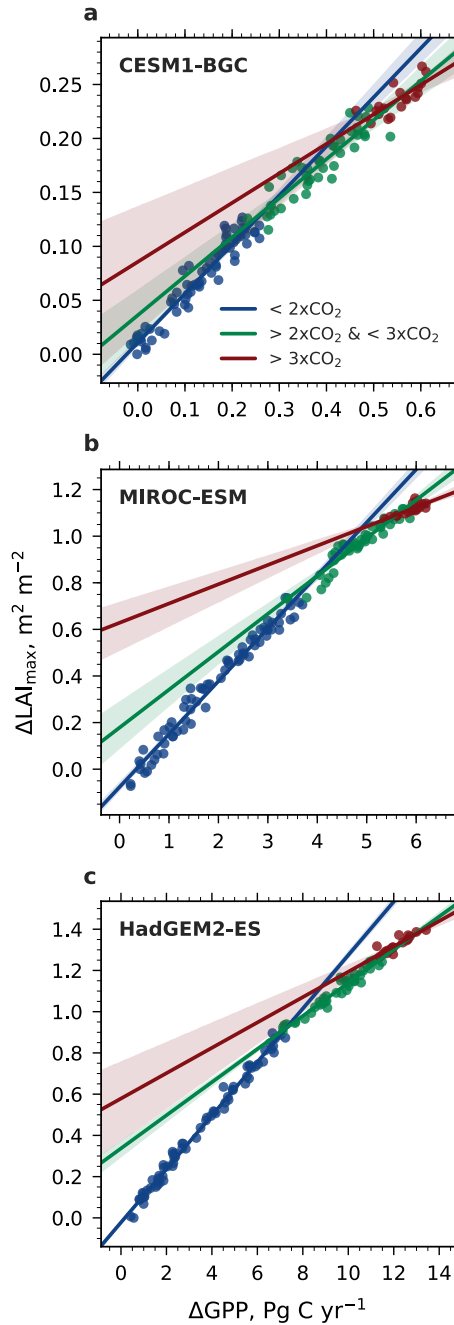
1  
2

3 **Figure 3.** Histograms and associated probability density functions (Gaussian kernel density estimation) of observed LAI<sub>max</sub> sensitivity to  
 4  $\omega$  at pixel scale for the northern high latitudinal band (> 60° N, data from AVHRR sensor). Blue color depicts the distribution of LAI<sub>max</sub>  
 5 sensitivities of all pixels and the red color for pixels with statistically significant (Mann-Kendall test,  $p < 0.1$ ) greening or browning trends  
 6 (the dashed lines denote the respective mean value). The green dashed line shows the mean value of 'greening' pixels only, whereas the  
 7 yellow dashed line shows the LAI<sub>max</sub> sensitivity to  $\omega$  for the entire northern high latitudinal belt.



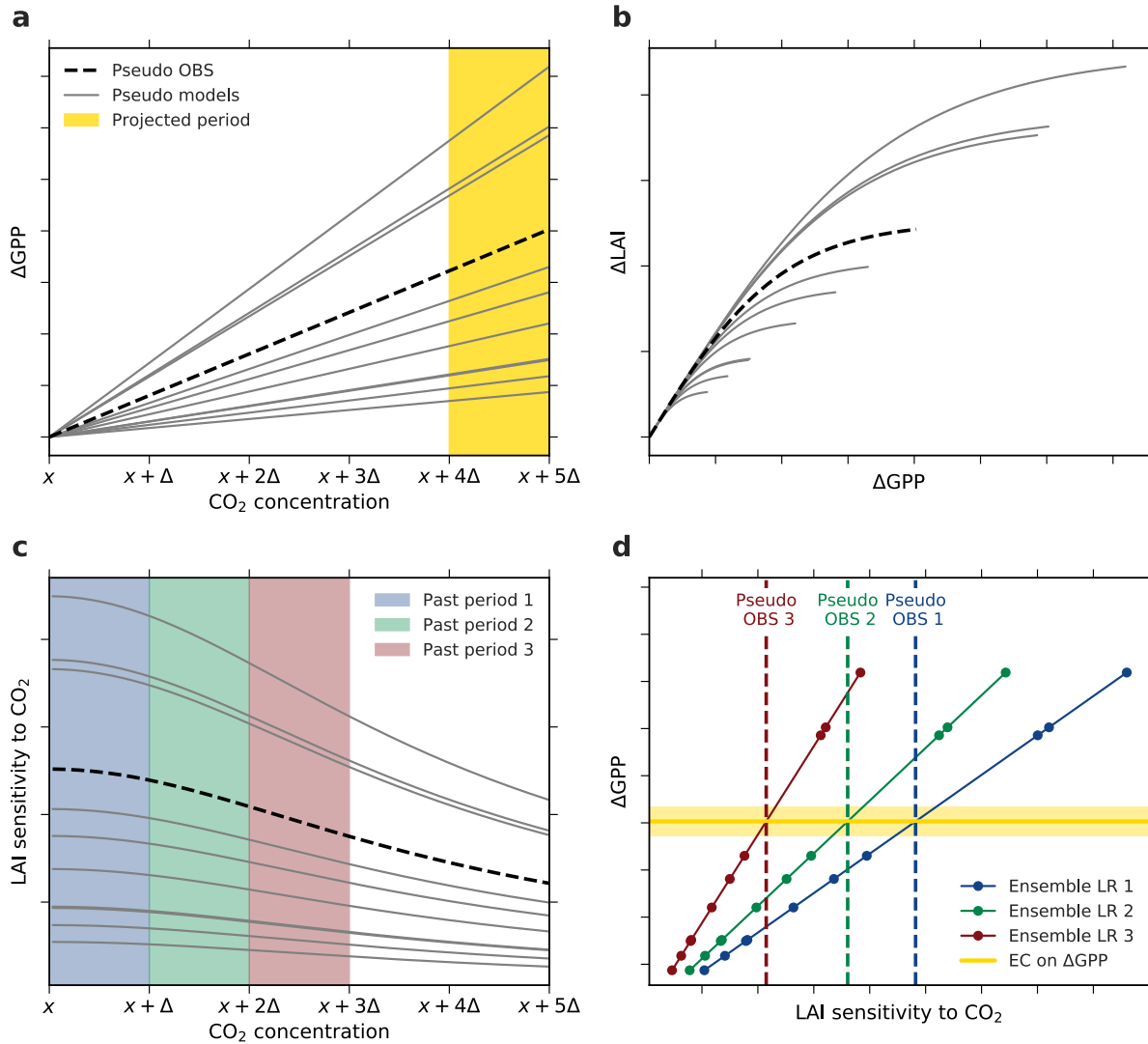
1  
2

3 **Figure 4.** Temporal variation of LAI<sub>max</sub> sensitivity to  $\omega$  in three selected CMIP5 models spanning the full range from low (CESM1-BGC,  
4 **a**), to closest-to-observations (MIROC-ESM, **b**), to high-end (HadGEM2-ES, **c**). The colored lines show LAI<sub>max</sub> sensitivity variations for  
5 moving windows of varying length of 15 (blue), 30 (green), and 45 (red) years over the historical period from 1860 to 2005.



1

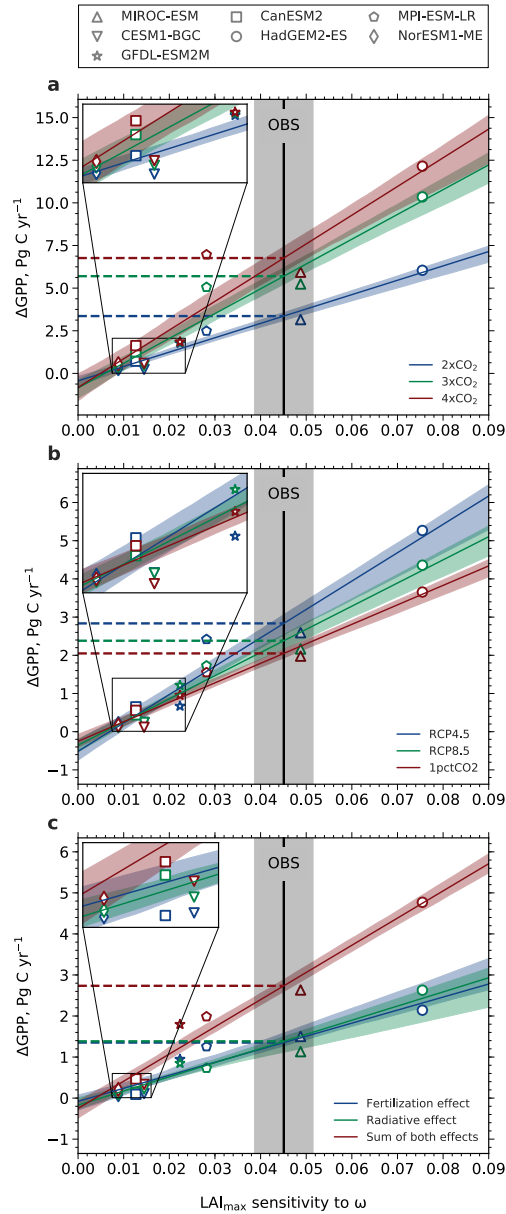
2 **Figure 5.** Correlation of  $\Delta\text{LAI}_{\text{max}}$  and  $\Delta\text{GPP}$  with increasing  $\text{CO}_2$  forcing, starting from a pre-industrial concentration of 280 ppm  
 3 ( $1\times 1\times\text{CO}_2$ ) to  $4\times 4\times\text{CO}_2$  (CMIP5 1pctCO2 simulations). Results are shown for three selected CMIP5 models spanning the full range of  
 4  $\text{LAI}_{\text{max}}$  sensitivity to  $\omega$ , low-end: CESM1-BGC (a), closest-to-observations: MIROC-ESM (b), and high-end: HadGEM2-ES (c). Blue col-  
 5 ored dots show the relation between  $1\times 1\times\text{CO}_2$  and  $2\times 2\times\text{CO}_2$ , green colored dots between  $2\times 2\times\text{CO}_2$  and  $3\times 3\times\text{CO}_2$ , and red colored dots  
 6 between  $3\times 3\times\text{CO}_2$  and  $4\times 4\times\text{CO}_2$ . The respective colored lines represent the best linear fit through those dots and the shading represents the  
 7 95% confidence interval.



1

2 **Figure 6.** Gedankenexperiment Thought experiment to examine the applicability of Emergent Constraints-EC analysis under the assumption  
3 of an idealized linear / nonlinear-non-linear behavior of the system (Case 3, Table A1). **a**, Changes in GPP relate linearly to changes in  $CO_2$   
4 concentration. The yellow band marks the projection period of interest, i.e. the period of  $CO_2$  concentration from  $x + 4\Delta$  to  $x + 5\Delta$ . **b**, The  
5 increment in LAI with increasing GPP is assumed to decrease with rising  $CO_2$  concentration (described by a hyperbolic tangent function).  
6 The parameterization in the linear and nonlinear-non-linear functions for pseudo observations (dashed black line) as well as models (solid  
7 grey lines) are determined randomly for each model. **c**, The diagnostic variable, LAI sensitivity to  $CO_2$ , is decreasing with increasing  $CO_2$   
8 as a consequence of the nonlinear-non-linear relation between  $\Delta GPP$  and  $\Delta LAI$ . The colored bands indicate three 'past' periods from  $x$  to  
9  $x + \Delta$  (blue),  $x + \Delta$  to  $x + 2\Delta$  (green), and  $x + 2\Delta$  to  $x + 3\Delta$  (red). **d**, Linear relationships among the pseudo model ensembles  
10 (Ensemble LR, colored lines) between LAI sensitivities to  $CO_2$  of the three past periods and  $\Delta GPP$  from the projected period. Colored dots  
11 mark different models and the dashed lines represent associated pseudo observations for the respective historical period. Yellow solid line  
12 depicts the constant Emergent Constraint-EC on projected  $\Delta GPP$  irrespective of the past period.





1

2 **Figure 7.** Linear relationships between historical sensitivity of  $LAI_{max}$  to  $\omega$  and absolute increase of GPP at different levels (a), different  
 3 time-rates (b) as well as effects of rising  $CO_2$  (c). The black solid line depicts the observational sensitivity including the standard error (grey  
 4 shading). Each CMIP5 model is represented by a distinct marker (legend at the top). The colored lines show the best linear fits including the  
 5 68% confidence interval estimated by bootstrapping across the model ensemble. The colored dashed lines indicate the derived constraints on  
 6  $\Delta GPP$ . a, Absolute changes in GPP at different levels of  $CO_2$ :  $2 \times CO_2$  (blue),  $3 \times CO_2$  (green), and  $4 \times CO_2$  (red). b, Absolute changes in  
 7 GPP for rising  $CO_2$  concentration from 380 to 535 ppm at different time-rates: RCP4.5 (90 yr, blue), RCP8.5 (45 yr, green), and 1pctCO2  
 8 (30 yr, red). c, Absolute changes in GPP due to the two disentangled effects of  $CO_2$  at  $2 \times CO_2$  in idealized simulations: Fertilization effect  
 9 (esmFixClim1, blue), radiative effect (esmFdbk1, green), and the sum of both effects (red).

1 **Table 1.** Coefficients of determination ( $R^2$ ) of LAI<sub>max</sub> sensitivity to  $\text{CO}_2$  for different large-scale aggregated regions. Data are from two  
 2 optical remote sensors of different time length, AVHRR (1982 – 2016) and MODIS (2000 – 2016). Asterisks denote non-significant values:  
 3 \*\* p > 0.1; \* p > 0.05.

<b>Correlation coefficient <math>R^2</math></b>	<b>AVHRR</b>	<b>MODIS</b>
<b>Biomes</b>		
Boreal forests	0.49	0.58
Temperate forests	0.47	0.81
Tropical forests	0.41	0.06**
Graslands	0.75	0.83
Croplands	0.75	0.8
Other	0.35	0.2*
<b>Latitudinal Bands</b>		
> 60° N/S	0.51	0.61
30° N/S – 60° N/S	0.67	0.83
30° S – 30° N	0.65	0.26
<b>Climate Space</b>		
cold dry	0.29	0.27
cold wet	0.49	0.4
cold humid	0.33	0.21*
warm dry	0.33	0.36
warm wet	0.37	0.18*
warm humid	0.25	0.12**
hot dry	0.08*	0.08**
hot wet	0.15	0.00**
hot humid	0.13	0.01**

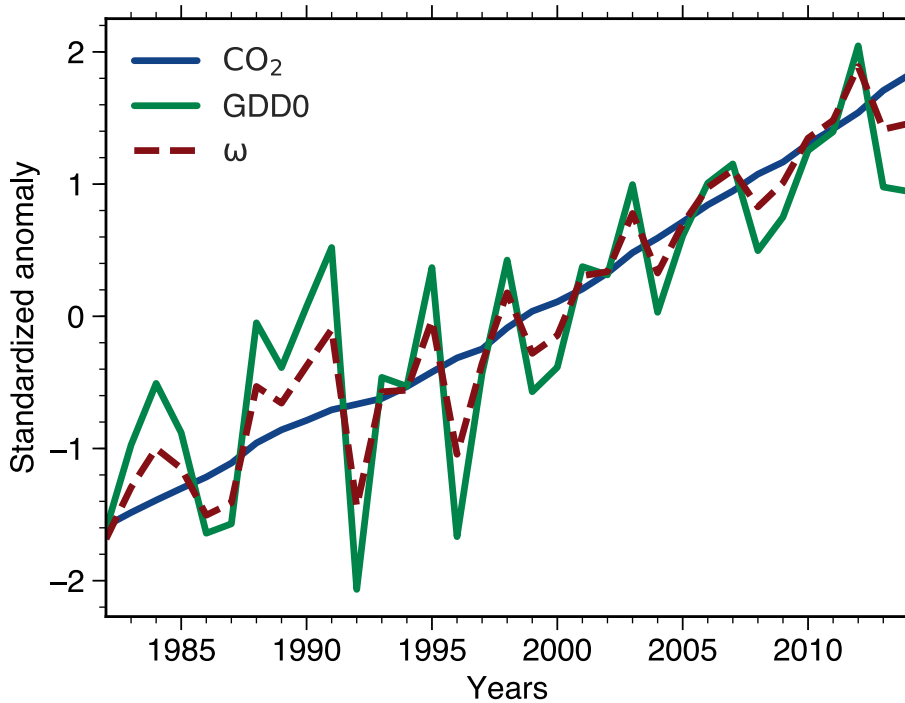
4

1 **Table 2.** Slopes ( $b$ ) and coefficients of determination ( $R^2$ ) for regression between changes of LAI<sub>max</sub> against changes in annual mean GPP  
2 at different atmospheric CO<sub>2</sub> levels in all available CMIP5 models (1pctCO2 simulation). Asterisks denote non-significant values: \*\*  $p >$   
3 0.1; \*  $p > 0.05$ .

	Correlation details	< 2xCO <sub>2</sub>		> 2xCO <sub>2</sub> & < 3xCO <sub>2</sub>		> 3xCO <sub>2</sub>	
		$b$	$R^2$	$b$	$R^2$	$b$	$R^2$
	MIROC-ESM	0.23	0.97	0.16	0.89	0.08	0.63
	CESM1-BGC	0.45	0.93	0.36	0.82	0.27	0.62
4	GFDL-ESM2M	0.37	0.89	0.04	0.07**	0.01	0.12**
	CanESM2	0.22	0.95	0.19	0.83	0.17	0.67
	HadGEM2-ES	0.13	0.99	0.08	0.96	0.06	0.78
	MPI-ESM-LR	0.13	0.94	0.09	0.78	0.04	0.51
	NorESM1-ME	0.26	0.94	0.2	0.77	0.09	0.27

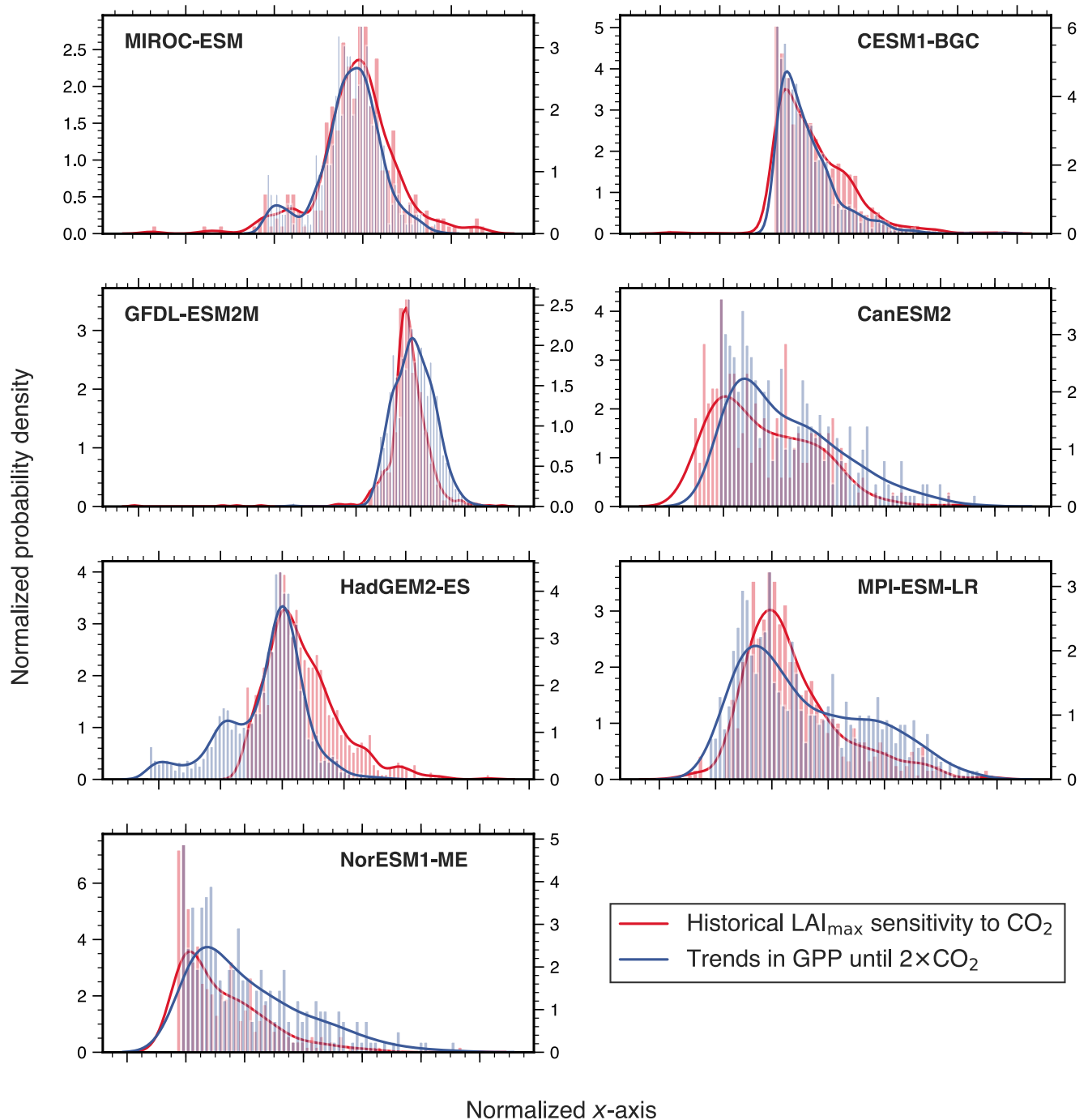
1 **Table 3.** Coefficients of determination ( $R^2$ ) of the emergent linear relationships in Figure 7 (asterisks denote non-significant values: \*\* p >  
2 0.1; \* p > 0.05). **Emergent Constraints** ECs on  $\Delta$ GPP (upper and lower bound of uncertainty in square brackets) for different atmospheric  
3 CO<sub>2</sub> levels and fully-coupled as well as idealized setups. The rightmost column shows the increase of  $\Delta$ GPP for an increment of  $1 \times \text{CO}_2$ .  
4 The lowermost section compares EC estimates of  $\Delta$ GPP for equivalent changes in CO<sub>2</sub> concentration (CO<sub>2</sub> rises from 380 to 535 ppm), but  
5 for different time-rates.

	$R^2$	EC $\Delta$ GPP estimate (Pg C yr <sup>-1</sup> )	EC $\Delta$ GPP for $\Delta 1 \times \text{CO}_2$ (Pg C yr <sup>-1</sup> )
<b>2xCO<sub>2</sub></b>			
Fully coupled (1pctCO2)	0.96	3.36 [3.15, 3.56]	–
CO <sub>2</sub> fertilization only (esmFixClim1)	0.88	1.35 [1.29, 1.62]	–
Radiative effect only (esmFdbk1)	0.94	1.38 [1.13, 1.51]	–
Sum of both effects (esmFixClim1 + esmFdbk1)	0.95	2.74 [2.6, 2.9]	–
<b>3xCO<sub>2</sub></b>			
Fully coupled (1pctCO2)	0.93	5.7 [5.26, 6.16]	2.34
CO <sub>2</sub> fertilization only (esmFixClim1)	0.92	2.15 [2.02, 2.37]	0.79
Radiative effect only (esmFdbk1)	0.98	2.53 [2.3, 2.66]	1.15
6 Sum of both effects (esmFixClim1 + esmFdbk1)	0.96	4.68 [4.38, 4.97]	1.94
<b>4xCO<sub>2</sub></b>			
Fully coupled (1pctCO2)	0.88	6.76 [6.08, 7.53]	1.06
CO <sub>2</sub> fertilization only (esmFixClim1)	0.88	2.42 [2.23, 2.74]	0.28
Radiative effect only (esmFdbk1)	0.97	3.06 [2.83, 3.2]	0.53
Sum of both effects (esmFixClim1 + esmFdbk1)	0.95	5.49 [5.09, 5.85]	0.81
<b>380 – 535 ppm CO<sub>2</sub></b>			
Slow increase in <u>CO<sub>2</sub></u> (RCP4.5)	0.93	2.84 [2.54, 3.08]	–
Medium-fast increase in <u>CO<sub>2</sub></u> (RCP8.5)	0.96	2.38 [2.18, 2.55]	–
Rapid increase in <u>CO<sub>2</sub></u> (1pctCO2)	0.96	2.05 [1.94, 2.16]	–



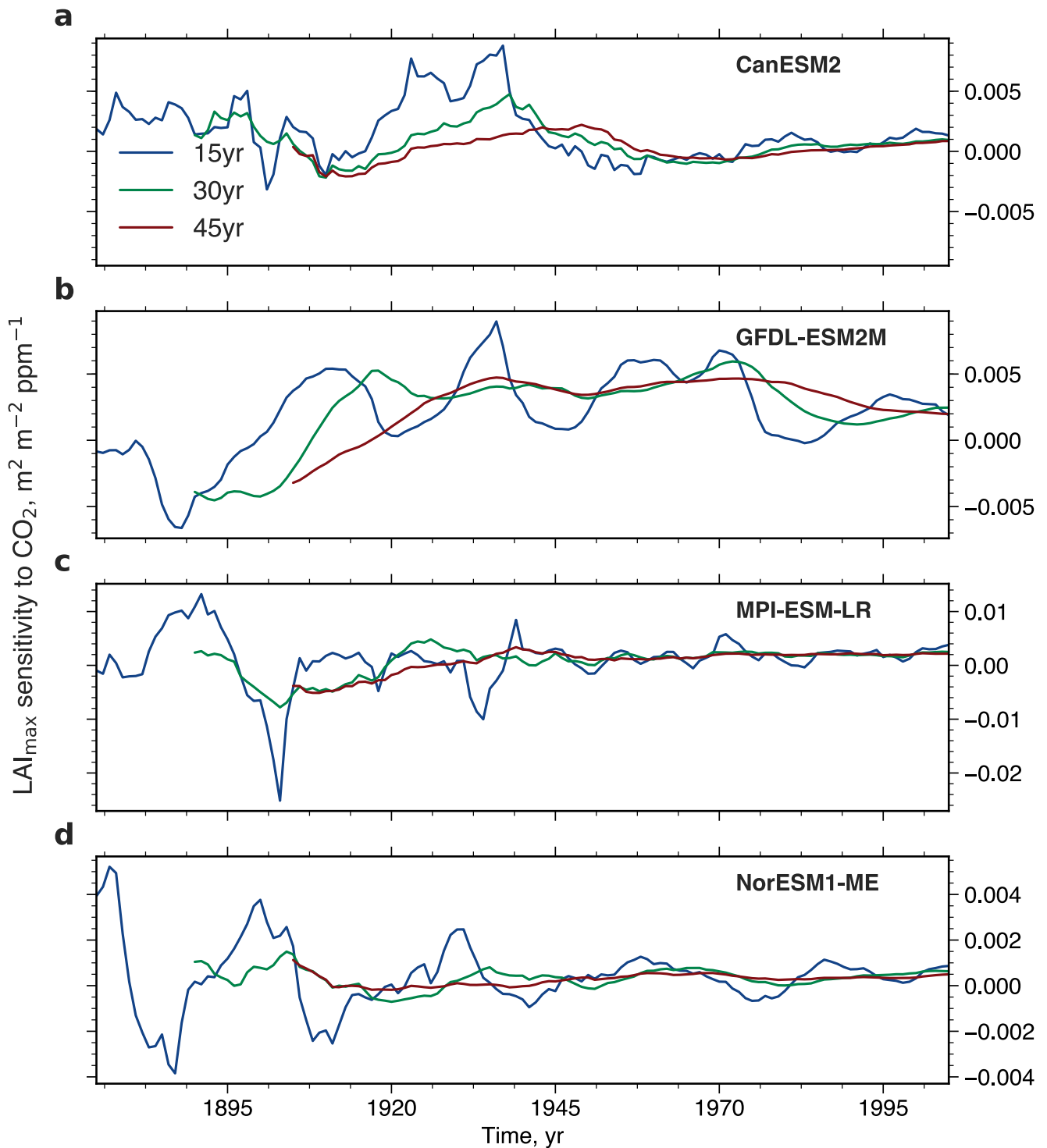
1

2 **Figure A1.** Gedankenexperiment to examine the applicability of the Emergent Constraints analysis  
 3 assuming an idealized linear / linear behavior of the system (Case 1, Table A1). **a.** Changes in GPP relate linearly to changes in annual  
 4 averaged atmospheric CO<sub>2</sub> concentration. The yellow band marks the projection period of interest, i.e. the period of concentration from  
 5  $x + 4\Delta$  to  $x + 5\Delta$ . **b.** Changes in LAI relate linearly to changes in GPP. The parameterization in the linear functions for pseudo  
 6 observations (dashed black blue solid line) as well as models (solid grey lines) are determined randomly for each model. **c.** The diagnostic  
 7 variable, LAI sensitivity to, remains constant with increasing as a consequence of the overall linear characteristics of the system. The colored  
 8 bands indicate three 'past' periods from  $x$  to  $x + \Delta$  area-weighted averaged GDD0 for NHL (blue),  $x + \Delta$  to  $x + 2\Delta$  (green solid line),  
 9 and  $x + 2\Delta$  to  $x + 3\Delta$  their leading principal component  $\omega$  (red). **d.** Linear relationships among the pseudo-model ensembles (Ensemble  
 10 LR 1-3 on top of each other, red) between LAI sensitivity to of the three past periods and  $\Delta$ GPP from the projected period. Red dots mark  
 11 different models and the dashed line represents associated pseudo- in observations for all three historical periods. Yellow solid line depicts the  
 12 constant Emergent Constraint on projected  $\Delta$ GPP irrespective of the past period.



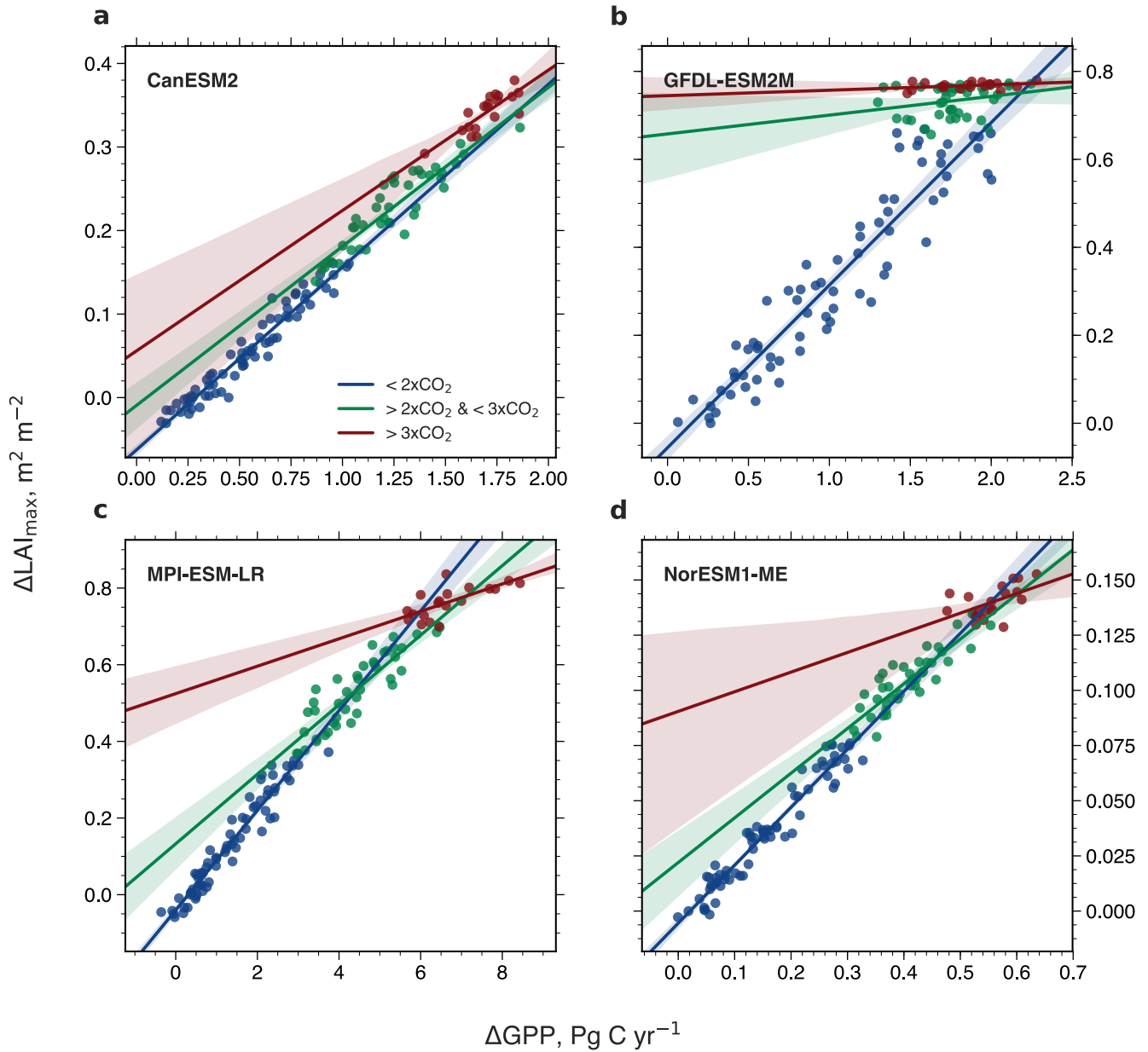
1  
2

3 **Figure A2.** Similar pixel distribution of predictor and predictand in each model, except HadGEM2-ES. Histograms and associated probability  
 4 density functions (Gaussian kernel density estimation) of LAI sensitivity to  $\omega$  (red, left y-axis, historical simulations) and temporal trends  
 5 in GPP (blue, right y-axis, 1pctCO<sub>2</sub>, until 2×CO<sub>2</sub>) for NHL are shown for all CMIP5 models. Only significant pixels are included  
 6 (Mann-Kendall test,  $p < 0.1$ ). To obtain comparability between the distributions, the x-axis was normalized and has only qualitative meaning.



1  
2

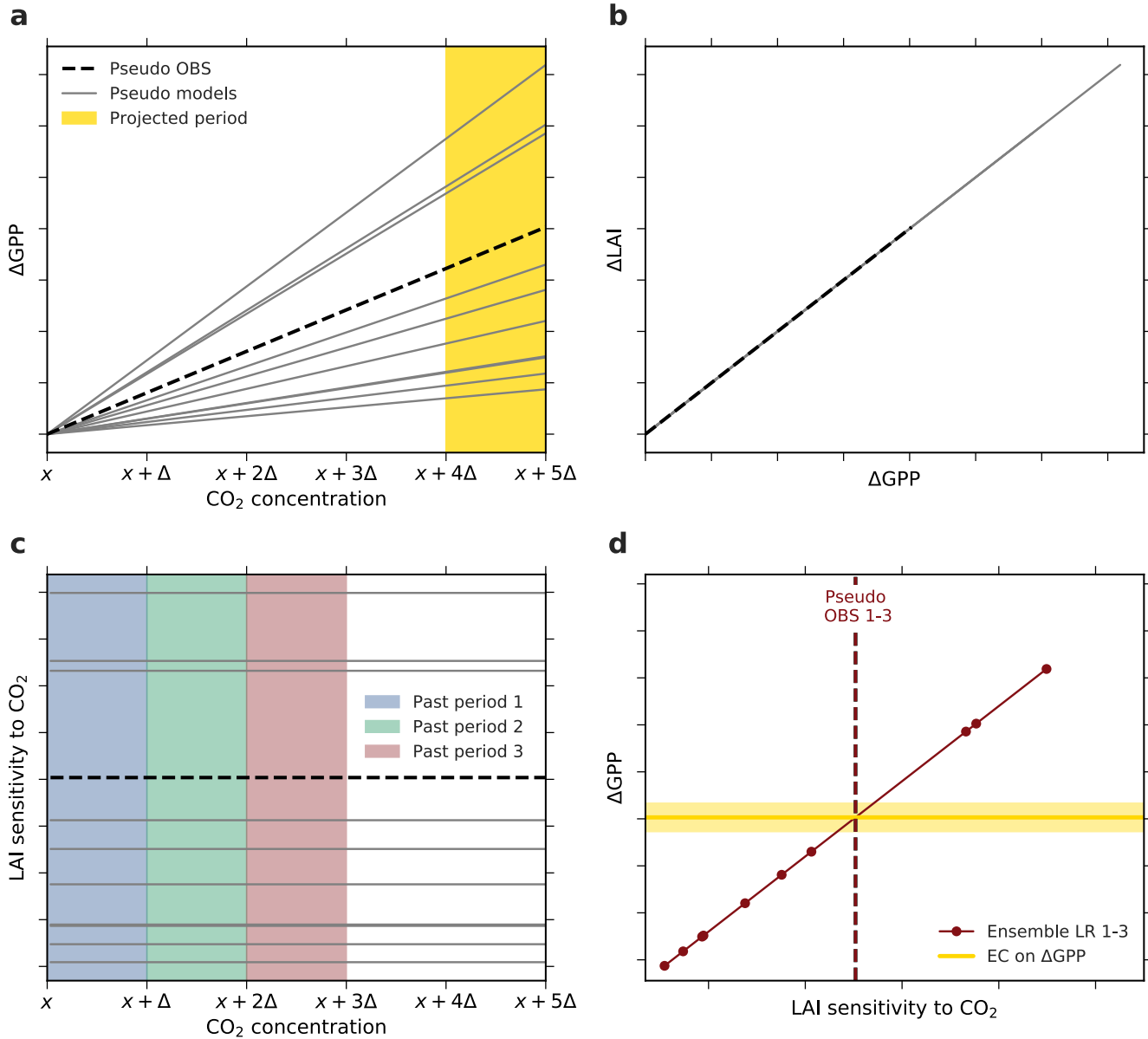
3 **Figure A3.** Temporal variation of  $LAI_{max}$  sensitivity to  $\omega$  in four CMIP5 models analogous to Fig. 4. The colored lines show  $LAI_{max}$   
 4 sensitivity variations for moving windows of varying length of 15 (blue), 30 (green), and 45 (red) years over the historical period from 1860  
 5 to 2005.



1  
2

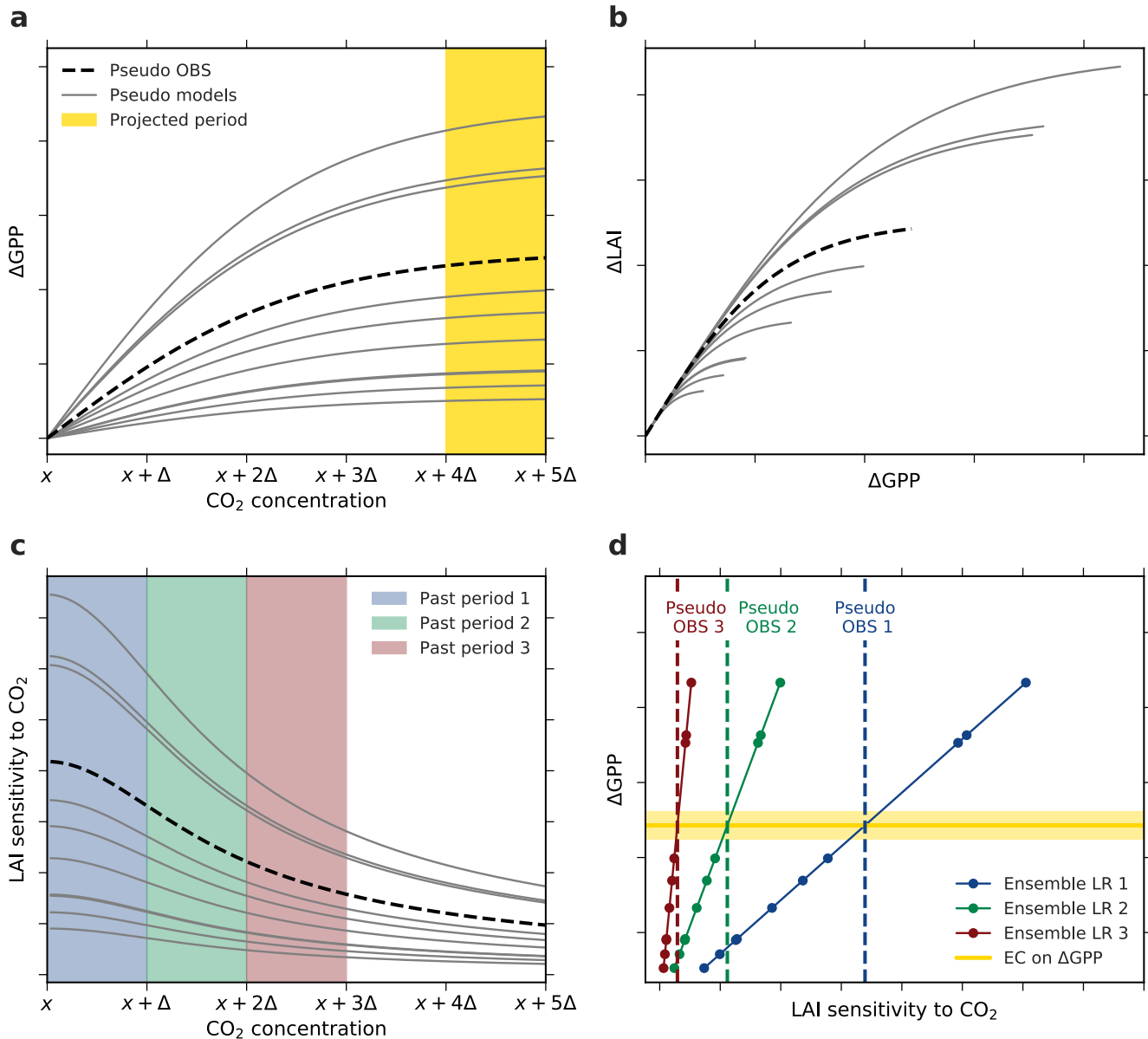
3 **Figure A4.** Correlation of  $\Delta\text{LAI}_{\text{max}}$  and  $\Delta\text{GPP}$  with increasing  $\text{CO}_2$  forcing, starting from a pre-industrial concentration of 280 ppm  
 4 ( $1\times\text{CO}_2$ ) to  $4\times\text{CO}_2$  (CMIP5 1pctCO2 simulations). Results are shown for four CMIP5 models analogous to Fig. 5. Blue colored dots show  
 5 the relation between  $1\times\text{CO}_2$  and  $2\times\text{CO}_2$ , green colored dots between  $2\times\text{CO}_2$  and  $3\times\text{CO}_2$ , and red colored dots between  $3\times\text{CO}_2$  and  $4\times\text{CO}_2$ .  
 6 The respective colored lines represent the best linear fit through those dots and the shading represents the 95% confidence interval.





1  
2

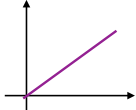
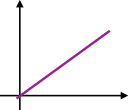
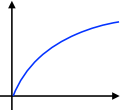
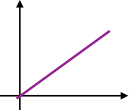
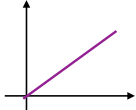
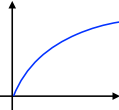
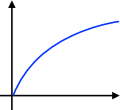
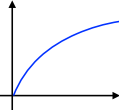
3 **Figure A5.** Thought experiment to examine the applicability of the EC analysis assuming an idealized linear / linear behavior of the system  
 4 (Case 1, Table A1). **a**, Changes in GPP relate linearly to changes in  $CO_2$  concentration. The yellow band marks the projection period  
 5 of interest, i.e. the period of  $CO_2$  concentration from  $x + 4\Delta$  to  $x + 5\Delta$ . **b**, Changes in LAI relate linearly to changes in GPP. The  
 6 parameterization in the linear functions for pseudo observations (dashed black line) as well as models (solid grey lines) are determined  
 7 randomly for each model. **c**, The diagnostic variable, LAI sensitivity to  $CO_2$ , remains constant with increasing  $CO_2$  as a consequence of the  
 8 overall linear characteristics of the system. The colored bands indicate three 'past' periods from  $x$  to  $x + \Delta$  (blue),  $x + \Delta$  to  $x + 2\Delta$   
 9 (green), and  $x + 2\Delta$  to  $x + 3\Delta$  (red). **d**, Linear relationships among the pseudo model ensembles (Ensemble LR 1-3 on top of each other,  
 10 red) between LAI sensitivity to  $CO_2$  of the three past periods and  $\Delta GPP$  from the projected period. Red dots mark different models and the  
 11 dashed line represents associated pseudo observations for all three historical periods. Yellow solid line depicts the constant EC on projected  
 12  $\Delta GPP$  irrespective of the past period.



1  
2

3 **Figure A6. Gedankenexperiment** Thought experiment to examine the applicability of the **Emergent Constraints-EC** analysis assuming an  
 4 idealized **nonlinear-non-linear / nonlinear-non-linear** behavior of the system (Case 4, Table A1). **a**,  $\Delta GPP$  decreases with increasing  $CO_2$   
 5 concentration (described by a hyperbolic tangent function). The yellow band marks the projected period of interest, i.e. the period of  $CO_2$   
 6 concentration from  $x + 4\Delta$  to  $x + 5\Delta$ . **b**, Also  $\Delta LAI$  decreases with increasing GPP (described by a hyperbolic tangent function).  
 7 The parameterization in the hyperbolic tangent functions for pseudo observations (dashed black line) as well as models (solid grey lines) are  
 8 determined randomly for each model. **c**, The diagnostic variable, LAI sensitivity to  $CO_2$ , is decreasing with increasing  $CO_2$  as a consequence  
 9 of the overall saturating characteristics of the system. The colored bands indicate three 'past' periods from  $x$  to  $x + \Delta$  (blue),  $x + \Delta$  to  
 10  $x + 2\Delta$  (green), and  $x + 2\Delta$  to  $x + 3\Delta$  (red). **d**, Linear relationships among the pseudo model ensembles (Ensemble LR, colored lines)  
 11 between LAI sensitivity to  $CO_2$  of the three past periods and  $\Delta GPP$  from the projected period. Colored dots mark different models and  
 12 the dashed lines represent associated pseudo observations for respective historical period. Yellow solid line depicts the constant **Emergent**  
 13 **Constraint-EC** on projected  $\Delta GPP$  irrespective of the past period.

- 1 **Table A1.** Overview of four possible cases of interaction between forcing, non-observable and observable identified in the
- 2 **Gedankenexperiment**thought experiment: All linear, all **nonlinear**non-linear, and two mixed cases.

Different assumptions	$\frac{d[\text{non-observable}]}{d[\text{forcing}]}$ , e.g. $\frac{d[\text{GPP}]}{d[\text{CO}_2]}$	$\frac{d[\text{observable}]}{d[\text{non-observable}]}$ , e.g. $\frac{d[\text{LAI}]}{d[\text{GPP}]}$
1	linear 	linear 
2	<b>nonlinear</b> <u>non-linear</u> 	linear 
3	linear 	<b>nonlinear</b> <u>non-linear</u> 
4	<b>nonlinear</b> <u>non-linear</u> 	<b>nonlinear</b> <u>non-linear</u> 

4